Nonperturbative evaluation of some QED contributions to the muonic hydrogen $n = 2$ Lamb shift and hyperfine structure

P. Indelicato[*]

Laboratoire Kastler Brossel, École Normale Supérieure, CNRS, Université Pierre et Marie Curie, Paris 6,
4 place Jussieu, F-75252 Paris CEDEX 05, France

The largest contributions to the $n = 2$ Lamb shift, fine structure interval and $2s$ hyperfine structure of muonic hydrogen are calculated by accurate numerical evaluations of the Dirac equation rather than by a perturbation expansion in powers of $1/c$, in the framework of nonrelativistic quantum electrodynamics. Previous calculations and the validity of the perturbation expansion for light elements are confirmed. The dependence of the various effects on the nuclear size and model are studied.

I. INTRODUCTION

Despite many years of study, the proton charge radius has remained relatively poorly known. It has been derived from measurements in electron-proton collisions [1,2] or from the high-precision spectroscopy of hydrogen [3–10] as described in the CODATA report in Ref. [11]. Tests of fundamental physics based on the progress in the accuracy of the spectroscopy of hydrogen and deuterium have been limited by the lack of an accurate value for the proton radius. Moreover, the values for the proton radius obtained by different methods or different analyses of the existing experiments are spread over a range larger than the uncertainty quoted for the individual results. Two recent measurements have resulted in a puzzle. The accurate determination of the $2S$ Lamb shift by laser spectroscopy in muonic hydrogen provides a proton size with a ten times smaller uncertainty than any previous value and it differs by *five* standard deviations from the 2006 CODATA value [12]. At the same time, a new, improved determination of the charge radius by electron scattering, performed at Mainz with the Mainz Microtron (MAMI), provides a value in good agreement with the value from hydrogen and deuterium spectroscopy [13,14]. Taking into account improved theory in hydrogen and deuterium and the MAMI measurement lead the recently released 2010 adjustment [15,16] to differ by 6.9 standard deviations between the proton radius obtained from muonic hydrogen.

Many papers have been published in the last year, trying to solve this puzzle. A few dealt with the calculation of the $n = 2$ level energies in muonic hydrogen. Several others are concerned with the effect of the internal structure of the proton on these energies [17–28]. Others look at exotic phenomenon beyond the standard model [29–35].

Many contributions to the Lamb shift, fine, and hyperfine structures of muonic hydrogen have been evaluated over the years; the results are summarized in Refs. [36–41] and in a recent book by Eides *et al.* [42]. Most of these calculations were done in the framework of nonrelativistic QED. The wave function and operators were expanded in powers of the fine structure constant, and the contributions were obtained by

perturbation theory. Hylton [43] showed that the perturbation calculation of the finite size correction to the vacuum polarization in heavy elements gives incorrect results. Since a bound muon is closer to the nucleus than a bound electron by a factor of $m_\mu/m_e \approx 207$, its Bohr radius is slightly smaller than the Compton wavelength of the electron $\lambda_C = \hbar/m_e c$ by a factor of $m_e/\alpha\, m_\mu \approx 137/207$ ($\alpha \approx 1/137.036$ is the fine structure constant, m_e and m_μ the electron and muon mass, respectively). The Compton wavelength is the scale of QED corrections, and for the $2S$ level, the muon wave-function mean radius is only 2.6 times larger than the electron Compton wavelength.

It is thus worthwhile to reconsider the largest corrections that contribute to the $2S$ Lamb shift in muonic hydrogen using nonperturbative methods. In the present work, we use the latest version of the MCDF code of Desclaux and Indelicato [44], which is designed to calculate the properties of exotic atoms [45], to evaluate the exact contribution of the electron Uehling potential with Dirac wave functions including the finite nuclear size. In the same way, we calculate the Källén and Sabry contribution.

Throughout this paper we will use QED units, $\hbar = 1$, $c = 1$. The electric charge is given by $e^2 = 4\pi\alpha$.

II. NUMERICAL EVALUATION OF THE DIRAC EQUATION WITH REALISTIC NUCLEAR CHARGE DISTRIBUTION MODELS

A. Evaluation by the numerical solution of the Dirac equation

We calculate higher-order finite size correction, starting from the Dirac equation with reduced mass, as techniques for the accurate numerical solution of the Dirac equation in a Coulomb potential have been developed over a period of many years within the framework of the multiconfiguration Dirac-Fock (MCDF) method for the atomic many-body problem [46–49].

The Dirac equation is written as

$$[\boldsymbol{\alpha} \cdot \boldsymbol{p} + \beta\mu_r + V_N(\boldsymbol{r})]\Phi_{n\kappa\mu}(\boldsymbol{r}) = \mathcal{E}_{n\kappa\mu}\Phi_{n\kappa\mu}(\boldsymbol{r}), \qquad (1)$$

where $\boldsymbol{\alpha}$ and β are the Dirac 4×4 matrices, $V_N(\boldsymbol{r})$ is the Coulomb potential of the nucleus, $\mathcal{E}_{n\kappa\mu}$ is the atom total energy,

---

*paul.indelicato@spectro.jussieu.fr

and Φ is a one-electron Dirac four-component spinor

$$\Phi_{n\kappa\mu}(\boldsymbol{r}) = \frac{1}{r}\left[\begin{array}{c} P_{n\kappa}(r)\,\chi_{\kappa\mu}(\theta,\phi) \\ i\,Q_{n\kappa}(r)\,\chi_{-\kappa\mu}(\theta,\phi) \end{array}\right], \tag{2}$$

in which $\chi_{\kappa\mu}(\theta,\phi)$ is the two-component Pauli spherical spinor [47], n is the principal quantum number, κ is the Dirac quantum number, and μ is the eigenvalue of J_z. This reduces, for a spherically symmetric potential, to the differential equation

$$\left[\begin{array}{cc} V_N(r) & -\frac{d}{dr}+\frac{\kappa}{r} \\ \frac{d}{dr}+\frac{\kappa}{r} & V_N(r)-2\mu_r \end{array}\right]\left[\begin{array}{c} P_{n\kappa}(r) \\ Q_{n\kappa}(r) \end{array}\right] = E^D_{n\kappa\mu}\left[\begin{array}{c} P_{n\kappa}(r) \\ Q_{n\kappa}(r) \end{array}\right], \tag{3}$$

where $P_{n\kappa}(r)$ and $Q_{n\kappa}(r)$ are the large and small radial components of the wave function, respectively, κ is the Dirac quantum number, $E^D_{n\kappa\mu}$ is the binding energy, μ_r is the muon reduced mass, $\mu_r = m_\mu M_p/(m_\mu + M_p)$ (m_μ and M_p are the muon and proton masses).

The numerical solution of this equation has been implemented for many years in the multiconfiguration Dirac-Fock general matrix elements (MDFGME) code developed from the original MCDF code of Desclaux [49] to work with exotic atoms [45] and several different nuclear models, with improved accuracy and QED corrections [50–53]. Here I used the 2012 version of the MDFGME code.

In this version, a five-point predictor-corrector method (order h^7) is used to solve Eq. (3) numerically, on a linear mesh [49,53] defined as

$$t_n = \ln\left(\frac{r_n}{r_0}\right) + ar_n, \tag{4}$$

with $t_n = t_0 + nh$, and $r_0 > 0$ is the first point of the mesh, corresponding to $n = 0$. This immediately gives $t_0 = ar_0$. Equation (4) can be inverted to yield

$$\begin{aligned} r_n &= \frac{W(ar_0 e^{t_n})}{a}, \\ \frac{dr_n}{dt_n} &= \frac{W(ar_0 e^{t_n})}{a[1 + W(ar_0 e^{t_n})]}, \end{aligned} \tag{5}$$

where W is the Lambert (or product logarithm) function. The wave function and differential equation between 0 and r_0 are represented by a ten-term series expansion. For a point nucleus, the first point is usually given by $r_0 = 10^{-2}/Z$ and $h = 0.025$. Here we use values down to $r_0 = 10^{-7}/Z$ and $h = 0.002$ to obtain the best possible accuracy. For a finite charge distribution, the nuclear boundary is fixed at the value r_N, where N is large enough to obtain sufficient accuracy. The mean value of an operator $\mathcal{O}$ that gives the first-order contributions to the energy is calculated as

$$\begin{aligned} \Delta E_{\mathcal{O}} &= \int_0^\infty dr[P(r)^2 + Q(r)^2]\mathcal{O}(r) \\ &= \int_0^{r_0} dr[P(r)^2 + Q(r)^2]\mathcal{O}(r) \\ &\quad + \int_{r_0}^\infty dt\,\frac{dr}{dt}[P(r)^2 + Q(r)^2]\mathcal{O}(r) \end{aligned} \tag{6}$$

using 8- and 14-point integration formulas due to Roothaan. The two integration formulas provide the same result within nine decimal places.

B. Charge distribution models

For the proton charge distribution two models are extensively used. The first corresponds to a proton dipole (charge) form factor, the second is a Gaussian model. Here we also use uniform and Fermi charge distribution and fits to the experimental data [54,55]. The analytic distributions are parametrized so they provide the same mean-square radius R. Moments of the charge distribution are defined by

$$\langle r^n \rangle = 4\pi \int_0^\infty r^{2+n}\rho(r)dr, \tag{7}$$

where the nuclear charge distribution $\rho(r) = \rho_N(r)/(Ze)$ is normalized by

$$\int \rho(\vec{r})\,d\vec{r} = 4\pi \int_0^\infty \rho(r)r^2 dr = 1, \tag{8}$$

for a spherically symmetric charge distribution. The mean-square radius is $R = \sqrt{\langle r^2 \rangle}$.

The potential can be deduced from the charge density using the well-known expression

$$V_N(r) = -\frac{4\pi e}{r}\int_0^r du\,u^2 \rho_N(u) - 4\pi e \int_r^\infty du u \rho_N(u). \tag{9}$$

The exponential charge distribution and corresponding potential energy are written as

$$\begin{aligned} \rho_N(r) &= Ze\,\frac{e^{-\frac{r}{\xi}}}{8\pi\xi^3}, \\ V_N(r) &= -Ze^2\left(\frac{1 - e^{-\frac{r}{\xi}}}{r} - \frac{e^{-\frac{r}{c}}}{2\xi}\right), \\ \langle r^n \rangle &= \frac{(n+2)!\,\xi^n}{2}, \end{aligned} \tag{10}$$

which gives $\xi = \frac{R}{2\sqrt{3}}$. The Gaussian charge distribution and potential are given by

$$\begin{aligned} \rho_N(r) &= Ze\,\frac{e^{-(\frac{r}{\xi})^2}}{\pi^{3/2}\xi^3}, \\ V_N(r) &= -Ze^2\,\frac{\mathrm{erf}(\frac{r}{\xi})}{r}, \\ \langle r^n \rangle &= \frac{2\Gamma(\frac{n+3}{2})\xi^n}{\sqrt{\pi}}, \end{aligned} \tag{11}$$

where erf is the error function and $\xi = \sqrt{\frac{2}{3}}R$. Other similar expressions for the two above models can be found in Ref. [56].

The electric form factor, corresponding to the interaction as depicted in Fig. 1, is related to the charge distribution by

$$G_E(\vec{Q}^2) = \int d\boldsymbol{r}\,e^{-i\boldsymbol{q}\cdot\boldsymbol{r}}\rho(\boldsymbol{r}). \tag{12}$$

$$-ie\gamma_\mu$$

$$-i\frac{g_{\mu\nu}}{q^2}$$

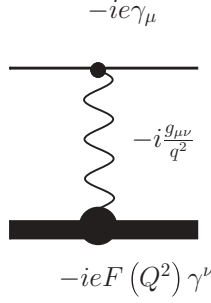$$-ieF\left(Q^2\right)\gamma^\nu$$

FIG. 1. Electromagnetic interaction between a lepton (narrow line) and a nucleon (bold line). The Feynman diagrams presented in the figures are realized with JAXODRAW.

For the exponential model this leads to

$$G_E(\vec{Q}^2) = \frac{1}{\left(1 + \frac{R^2 q^2}{12}\right)^2} \approx 1 - \frac{R^2}{6}q^2 + \frac{R^4}{48}q^4 + \cdots, \tag{13}$$

while for the Gaussian model one has

$$G_E(\vec{Q}^2) = e^{-\frac{1}{6}R^2 q^2} \approx 1 - \frac{R^2}{6}q^2 + \frac{R^4}{72}q^4 + \cdots. \tag{14}$$

The two models have an identical slope $R^2/6$ as functions of q^2 for $q \to 0$ as expected (see, e.g., [57]).

In 1956, Zemach introduced an electromagnetic form factor, useful for evaluating the hyperfine structure (HFS) energy correction

$$\rho_{em}(\boldsymbol{r}) = \int \rho(\boldsymbol{r}-\boldsymbol{u})\mu(\boldsymbol{u})d\boldsymbol{u}, \tag{15}$$

where $\mu(\boldsymbol{u})$ is the magnetic moment density. Both $\mu(\boldsymbol{u})$ and ρ_{em} are normalized to unity as in Eq. (8). The Zemach radius is given by

$$R_{\mathbf{Z}} = \langle r_{\mathbf{Z}} \rangle = \int r\rho_{em}(\boldsymbol{r})d\boldsymbol{r}. \tag{16}$$

The Zemach's radius can be written in momentum space as [58,59]

$$R_{\mathbf{Z}} = \frac{-4}{\pi} \int dq \frac{1}{q^2} \left(G_E(\vec{Q}^2) \frac{G_{\mathrm{M}}(\vec{Q}^2)}{1+\kappa_p} - 1 \right), \tag{17}$$

where κ_p is the proton anomalous magnetic moment, and G_M is normalized so that $G_M(0) = 1 + \kappa_p$. The exponential and Gaussian models enable us to obtain analytic results for R_Z as a function of the charge and magnetic moment radii R and R_M. Using Eqs. (13) or (14) for the exponential or Gaussian model, and Eq. (17), we get, respectively,

$$R_{\mathbf{Z}}^{\mathrm{Exp.}} = \frac{3R^4 + 9R^3 R_M + 11R^2 R_M^2 + 9R R_M^3 + 3R_M^4}{2\sqrt{3}(R + R_M)^3} \tag{18}$$

$$R_{\mathbf{Z}}^{\mathrm{Gauss}} = 2\sqrt{\frac{2}{3\pi}}\sqrt{R^2 + R_M^2}. \tag{19}$$

Another useful quantity, which appears in the estimation of the finite size correction to vacuum polarization, is the third Zemach's moment

$$\langle r^3 \rangle_{(2)} = \int r^3 \rho_{(2)}(\boldsymbol{r})d\boldsymbol{r}, \tag{20}$$

where the convolved charge distribution is

$$\rho_{(2)}(\boldsymbol{r}) = \int \rho(\boldsymbol{r}-\boldsymbol{u})\rho(\boldsymbol{u})d\boldsymbol{u}. \tag{21}$$

This can be rewritten in the more convenient form [18,36], in the limit of large proton masses,

$$\langle r^3 \rangle_{(2)} = \frac{48}{\pi} \int dq \frac{1}{q^4} \left(G_E^2(\vec{Q}^2) - 1 + \frac{q^2}{3}R^2 \right). \tag{22}$$

It can be easily seen from Eqs. (13) or (14) that the expression is finite for $q \to 0$.

We now turn to more realistic models, based on the experiment. A recent analysis of the world's data on elastic electron-proton scattering and calculations of two-photon exchange effects provides an analytic expression for the electric form factors [55], given as

$$G_E(\vec{Q}^2) = \frac{1 + \sum_{i=0}^{2} a_i \tau^i}{1 + \sum_{j=0}^{4} b_j \tau^j}, \tag{23}$$

where $\tau = q^2/(4M_p)$. The a_i coefficients can be found in Table I of Ref. [55]. A second work [54] used a combination of several spectral functions, taking into account several resonances and continua like the 2π, $K\overline{K}$, and $\rho\pi$ continua. Here we use the fit resulting from the *superconvergence approach* from this work. This corresponds to a sum of 12 dipole-like functions, which are able to represent the experimental data with a reduced χ^2 of 1.8. A comparison of the electric form factor from both works is presented in Fig. 2. It is clear that both the experimental form factors and the dipole approximation with an identical radius are very close. We can obtain the charge radius and the next correction by performing an expansion in q of the experimental form factors. We get for [55]

$$G_E(\vec{Q}^2) \approx 1 - \frac{0.8503^2}{6}q^2 + \frac{0.8503^4}{43.3909}q^4 + \cdots, \tag{24}$$

and for [54]

$$G_E(\vec{Q}^2) \approx 1 - \frac{0.84995^2}{6}q^2 + \frac{0.84995^4}{38.793}q^4 + \cdots. \tag{25}$$
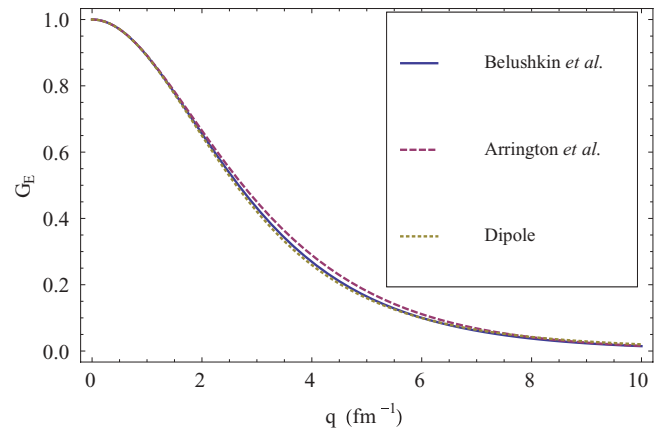

FIG. 2. (Color online) Comparison of the electric form factor from [54,55], with a dipole model with the same $R = 0.850$ fm as deduced from the experimental function.
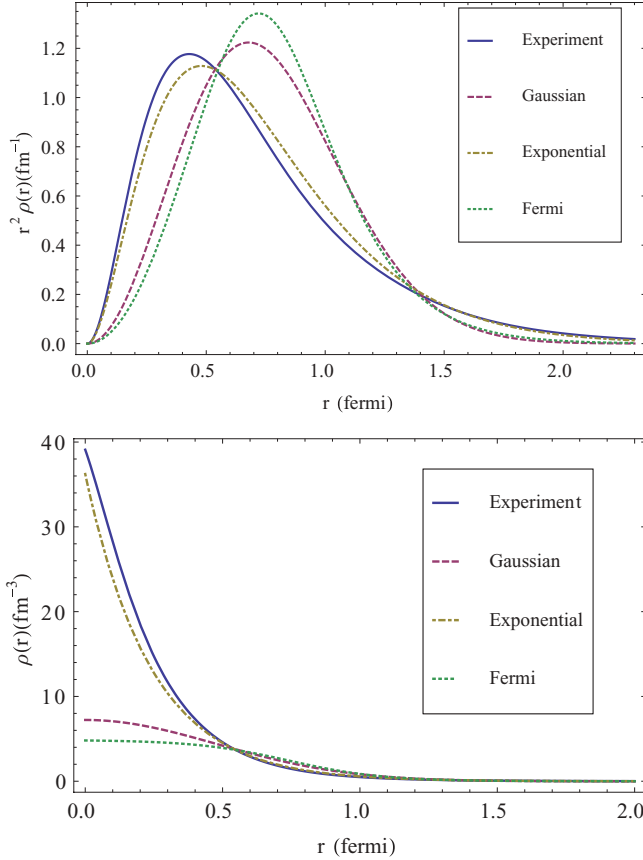
FIG. 4. Feynman diagrams corresponding to the full vacuum polarization contribution and expansion in $Z\alpha$. Diagram (a) corresponds to the Uehling potential [Eqs. (26) and (28)]. Diagram (b) corresponds to the Wichmann and Kroll correction. The double line represents a bound lepton wave function, the wavy line a Coulomb photon propagator. The single line corresponds to a free electron-positron (or muon-antimuon) pair. The gray circles correspond to the interaction with the nucleus.

FIG. 3. (Color online) Top: Charge densities $\rho(r)$ (fm^{-3}), bottom: charge densities $r^2\rho(r)$ (fm^{-1}) for the experimental fits in Ref. [55], compared to Gaussian, Fermi, and exponential models distributions. All models are calculated to have the same $R = 0.850$ fm RMS radius as deduced from the experimental function.

These expansions are very close to the one for a dipole form factor from Eq. (13).

To compare different charge density models, we have performed an analytic evaluation of the charge densities corresponding to [55], replacing Eq. (23) in Eq. (12) and performing the inverse Fourier transforms, to obtain the corresponding charge distribution, depending on the set of a coefficients. The corresponding densities are plotted and compared to the Fermi, Gaussian, and exponential models. Distances are converted from GeV to fm using $\hbar c = 0.1973269631$ GeV fm in the density obtained from the experiment. The charge distributions are compared in Fig. 3. We plotted both $\rho(r)$ and $\rho(r)r^2$ to reveal the differences at long and medium distances. The experimental charge density is rather different from all three analytic distributions, while, once multiplied by r^2, it is closer to the exponential distribution.

III. EVALUATION OF MAIN VACUUM POLARIZATION AND FINITE SIZE CORRECTION

The Feynman diagram corresponding to the Uehling approximation to the vacuum polarization correction is presented in Fig. 4(a). The evaluation of the vacuum polarization can be performed using standard techniques of (perturbative) nonrelativistic QED (NRQED) as described in Refs. [36,38].
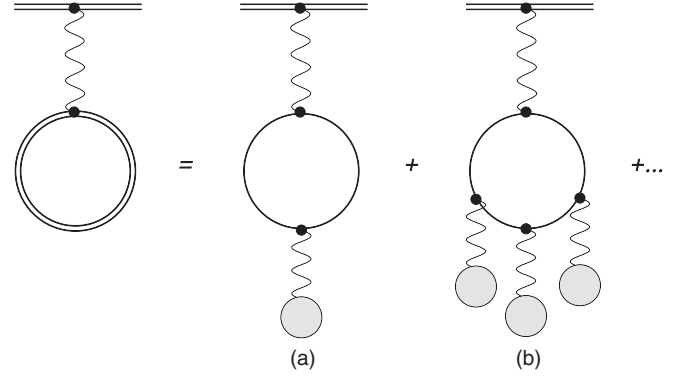
Here we use the analytic results of Klarsfeld [60] as described in Ref. [61] and the numerical solution of the Dirac equation from Sec. II. To obtain higher-order effects, we solve the Dirac equation in a combined potential resulting from the finite nuclear charge distribution and of the Uehling potential. The logarithmic singularity of the Uehling potential at the origin for a point charge cannot be easily incorporated in a numerical Dirac solver. In the case of a finite charge distributions, the singularity is milder, but great care must be exercised to obtain results accurate enough for our purpose.

For a point charge, the Uehling potential, which represents the leading contribution to the vacuum polarization, is expressed as [60,62,63]

$$V_{11}^{\text{pn}}(r) = -\frac{\alpha(Z\alpha)}{3\pi}\int_1^\infty dz\sqrt{z^2-1}\left(\frac{2}{z^2}+\frac{1}{z^4}\right)\frac{e^{-2m_e rz}}{r}$$
$$= -\frac{2\alpha(Z\alpha^2)}{3\pi}\frac{1}{r}\chi_1\left(\frac{2}{\lambda_e}r\right), \qquad (26)$$

where m_e is the electron mass, λ_e is the electron Compton wavelength, and the function χ_1 belongs to a family of functions defined by

$$\chi_n(x) = \int_1^\infty dz\, e^{-xz}\frac{1}{z^n}\left(\frac{1}{z}+\frac{1}{2z^3}\right)\sqrt{z^2-1}. \qquad (27)$$

The Uehling potential for a spherically symmetric charge distribution is expressed as [60]

$$V_{11}(r) = -\frac{2\alpha(Z\alpha)}{3}\frac{1}{r}\int_0^\infty dr'\, r'\rho(r')$$
$$\times\left[\chi_2\left(\frac{2}{\lambda_e}|r-r'|\right)-\chi_2\left(\frac{2}{\lambda_e}|r+r'|\right)\right]. \qquad (28)$$

The expression of the potential at the origin is given by

$$V_{11}(0) = -\frac{8\alpha(Z\alpha)}{3}\int_0^\infty dr'\, r'\rho(r')\chi_1\left(\frac{2}{\lambda_e}r'\right), \qquad (29)$$
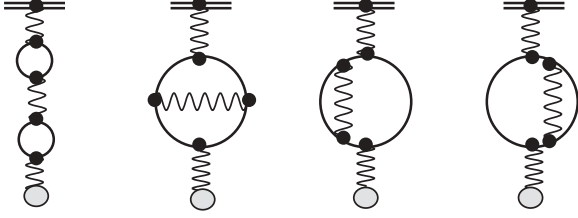
FIG. 5. Feynman diagrams included in the Källen and Sabry $V_{21}(r)$ potential [Eq. (32)]. See Fig. 4 for explanation of symbols.

while it behaves at large distances as [64]

$$V_{11}(r) = -\frac{2\alpha(Z\alpha)}{3\pi}\frac{1}{r}\left[\chi_1\left(\frac{2}{\lambda_e}r\right) + \frac{2}{3}\langle r^2\rangle\chi_{-1}\left(\frac{2}{\lambda_e}r\right) \right. \\ \left. + \frac{2}{15}\langle r^4\rangle\chi_{-3}\left(\frac{2}{\lambda_e}r\right) + \cdots\right] \quad (30)$$

using the moments of the charge distribution (7). The energy shift associated with the potential (26) or (28) in first-order perturbation is calculated as

$$\Delta E_{nl\kappa}^{11,pn} = \langle n,l,\kappa,\mu_r \,|V_{11}|\, n,l,\kappa,\mu_r\rangle \quad (31)$$

where $|n,l,\kappa,\mu_r\rangle$ is a wave-function solution of Eq. (1), which depends on the reduced mass. It was shown recently [65] that this method provides the correct inclusion of the vacuum polarization recoil correction at the Barker and Glover level [66]. Since we directly use relativistic functions, the other corrections described in Ref. [65] are automatically included.

IV. HIGHER-ORDER QED CORRECTIONS

A. Reevaluation of the Källèn and Sabry potential

The Källén and Sabry potential [67], is a fourth-order potential, corresponding to the diagrams in Fig. 5. The expression for this potential has also been derived in Refs. [68–71]. In the previous version of the MDFGME code, the Källèn and Sabry potential used was the one provided by the authors of [64], which is only accurate to three digits. The expression of this potential is for a point charge

$$V_{21}(r) = \frac{\alpha^2(Z\alpha)}{\pi^2 r}L_1\left(\frac{2}{\lambda_e}r\right), \quad (32)$$

where

$$L_1(r) = \int_1^\infty dt\, e^{-rt}\left\{\left(\frac{2}{3t^5} - \frac{8}{3t}\right)f(t) \right. \\ + \left(\frac{2}{3t^4} + \frac{4}{3t^2}\right)\sqrt{t^2-1}\ln[8t(t^2-1)] \\ + \sqrt{t^2-1}\left(\frac{2}{9t^6} + \frac{7}{108t^4} + \frac{13}{54t^2}\right) \\ \left. + \left(\frac{2}{9t^7} + \frac{5}{4t^5} + \frac{2}{3t^3} - \frac{44}{9t}\right)\ln(\sqrt{t^2-1}+t)\right\}, \quad (33)$$

and

$$f(t) = \int_t^\infty dx\left\{\frac{(3x^2-1)\ln(\sqrt{x^2-1}+x)}{x(x^2-1)} \right. \\ \left. - \frac{\ln[8x(x^2-1)]}{\sqrt{x^2-1}}\right\}. \quad (34)$$

The function $f(t)$ can be calculated analytically in term of the ln and dilogarithm functions. Blomqvist [72] has shown that $L_1(r)$ can be expressed as

$$L_1(r) = g_2(r)\ln^2(r) + g_1(r)\ln(r) + g_0(r), \quad (35)$$

and provided a series expansion of this function for small r. Fullerton and Rinker [64] provided polynomial approximations to the functions $g_i(r)$. Here we have numerically evaluated the function $L_1(r)$ to a very good accuracy, using MATHEMATICA. We then fitted the coefficients of polynomials for the function $g_i(r)$. The results are presented in Appendix A. For $x > 3$, we have used the functional form

$$L_1(r) = \frac{e^{-r}(a + b\sqrt{r} + cr + dr^{3/2} + er^2 + fr^{5/2})}{r^{7/2}}. \quad (36)$$

The coefficients are also given in Appendix A.

To obtain the finite nuclear size correction, we use the known expression for a spherically symmetric charge distribution [64]

$$V_{21}(r) = \frac{\alpha^2(Z\alpha)}{\pi^2 r}\int_0^\infty dr'r'\rho(r')\left[L_0\left(\frac{2}{\lambda_e}|r-r'|\right) \right. \\ \left. - L_0\left(\frac{2}{\lambda_e}|r+r'|\right)\right], \quad (37)$$

where

$$L_0(x) = -\int^x du\, L_1(u). \quad (38)$$

Using our approximation to $L_1(x)$ in Eqs. (35) and (36), we obtain the following approximate expressions for $L_0(x)$. For $x \leqslant 3$, the expression is very similar to the one for $L_1(x)$. One obtains

$$L_0(r) = rh_2(r)\ln^2(r) + rh_1(r)\ln(r) + h_0(r), \quad (39)$$

The expression for the functions h_i are given in Appendix B. For the asymptotic function, given for $x > 3$, we integrate directly Eq. (36), which yields [fixing the integration constant so that $L_0(r)$ is 0 at infinity]

$$L_0(r) = 41.1352787432251923 \\ - 5.1094977559522696[8.05074798111\mathrm{erf}(\sqrt{r}) \\ - 1.028091975364\mathrm{Ei}(-r) \\ + \frac{e^{-r}}{r^{5/2}}(-2.02809197536r^{3/2} + 4.54214815071r^2 \\ - 0.494718704003r + 0.98439728916\sqrt{r} \\ - 0.344009752879)] \quad (40)$$

where $\mathrm{Ei}(r)$ is the exponential integral.

V. NUMERICAL RESULTS

A. Finite size correction to the Coulomb contribution

Obtaining the accuracy required from the calculation on $E_{2\kappa\mu}^{D}$, which has a value of ≈ 632.1 eV, while the Lamb shift is ≈ 0.22 eV with an aim at better than 0.001 meV, is a very demanding task. For a point nucleus, we get exact degeneracy for the $2s$ and $2p_{1/2}$ Dirac energies. The best numerical accuracy was obtained generating the wave function on a grid with $r_0 = 2 \times 10^{-3}$ and $h = 2 \times 10^{-3}$. This corresponds to ≈ 8700 tabulation points for the wave function, with around 2800 points inside the proton. I checked that variations in r_0 and h do not change the final value. The main finite nuclear size effect on the $2p_{1/2}$–$2s$ energy separation comes from the sum of the Dirac energy splitting (the $2p_{1/2}$ and $2s$ levels are exactly degenerate for a point nucleus).

I evaluated the different quantities on a grid of proton sizes ranging from 0.3 to 1.2 fm, with steps of 0.025 fm (80 points). I also evaluated the contribution for the muonic hydrogen proton size and the CODATA 2010 proton size. The first few terms of the dependence of the relativistic energy on the moments of the charge distribution were given by Friar [56]. For a Gaussian charge distribution he finds for an s state

$$\Delta E^{\text{Coul.}} = a\langle r^2 \rangle + b\langle r^3 \rangle_{(2)} + c\langle r^2 \rangle^2$$
$$+ d\langle r^2 \rangle \langle \ln r \rangle + e\langle r^2 \rangle^2 \langle \ln r \rangle. \quad (41)$$

I use this as a guide to fit my numerical results.

As a first example a three-parameter fits provides

$$\Delta E_{2p_{1/2}-2s_{1/2}}^{\text{Coul.}}(R) = -5.19972\,R^2 + 0.0351289\,R^3$$
$$- 0.0000534235\,R^4\,\text{meV}. \quad (42)$$

A better fit is provided by

$$\Delta E_{2p_{1/2}-2s_{1/2}}^{\text{Coul.}}(R) = -5.19990R^2 + 0.0355905R^3$$
$$- 0.000488059R^4 + 0.000172334R^5$$
$$- 0.0000245051R^6\,\text{meV}. \quad (43)$$

Using a Friar functional form with only one $\ln R$ term, I obtain

$$\Delta E_{2p_{1/2}-2s_{1/2}}^{\text{Coul.}}(R) = -5.199365R^2 + 0.03466100R^3$$
$$+ 0.00007366037R^4 - 0.00001720960R^5$$
$$+ 1.198332 \times 10^{-6}R^6$$
$$+ 0.0002677236R^2\ln R\,\text{meV}. \quad (44)$$

The function with two logarithmic terms and close values of the Bayesian information criterion (BIC) and χ^2 criteria is given by

$$\Delta E_{2p_{1/2}-2s_{1/2}}^{\text{Coul.}}(R)$$
$$= -5.199337R^2 + 0.03458139R^3 + 0.0001092856R^4$$
$$+ 0.0002788380R^2\ln R - 0.00004957598R^4\ln R. \quad (45)$$

Criteria for the quality of the fit are plotted in Fig. 6. I use both the reduced χ^2 and a BIC to evaluate the improvement in the value when increasing the number of parameters [73]. We obtain a coefficient for R^2 which is -5.1999 meV/fm^2 and a coefficient for R^3 equal to 0.03559 meV/fm^3. Using our numerical solutions we also find -5.19972 meV/fm^2 and 0.032908 meV/fm^3 for the Gaussian model. Borie [40] found
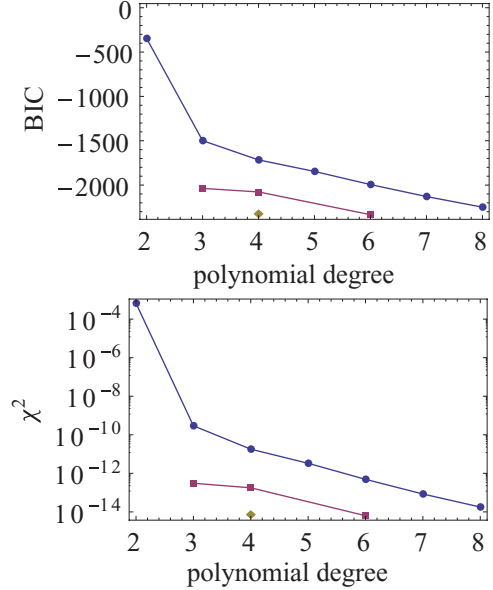

FIG. 6. (Color online) BIC criterium (top) and reduced χ^2 (bottom) as a function of the degree of the polynomial and of the logarithmic dependence used in the fit of the $2s - 2p_{1/2}$ Dirac energy difference as a function of R. Plotted quantities are dimensionless. •: Polynomial fit. ■: Polynomial and $R^2\ln R$ fit. ◆: Polynomial, $R^2\ln R$ and $R^4\ln R$ fit.

-5.1975 meV/fm^2 and 0.0347 meV/fm^3 for an exponential model, and 0.0317 meV/fm^3 for a Gaussian model, in reasonable agreement with the result presented here.

In the same way, I evaluated the finite size correction to the fine structure

$$\Delta E_{2p_{3/2}-2p_{1/2}}^{\text{Coul.}}(R) = 8.41563570 - 0.00005192R^2$$
$$+ 1.1818650 \times 10^{-7}R^3$$
$$- 1.19528126 \times 10^{-9}R^4\,\text{meV}. \quad (46)$$

The constant term is in perfect agreement with Borie's value 8.41564 meV [74] (Table 7).

It is interesting to explore at this stage the influence of the charge distribution shape on the Coulomb and vacuum polarization contribution. Friar and Sick [75] have evaluated the third Zemach moment from Eq. (20), using the proton-electron scattering data available in 2005. Using a model-independent analysis, they found $\langle r^3 \rangle_{(2)} = 2.71 \pm 0.13$ fm^3, leading to an energy shift of -0.0247 ± 0.0012 meV. Using the Fourier transform of the exponential (13) distribution in Eq. (22), I find

$$\langle r^3 \rangle_{(2)} = \frac{35\sqrt{3}R^3}{16} \approx 3.789R^3, \quad (47)$$

showing that $\langle r^3 \rangle_{(2)}$ is proportional to R^3 and justifying the fit in R^2 and R^3 performed to derive the coefficients above. Equation (47) is in exact agreement with the result that can be obtained from Eq. (15) in Ref. [17], but Eq. (16) in the same work is not correct (the denominator should be 256 not 64). The value obtained by Friar and Sick corresponds to $R = 0.894$ fm. In that case our energy shift is -0.0250 meV, in good agreement with the energy shift in Ref. [75]. In the

Gaussian model, I find

$$\langle r^3 \rangle_{(2)} = \frac{32R^3}{3\sqrt{3\pi}} \approx 1.960R^3, \tag{48}$$

leading to $R = 0.920$ fm and an energy shift of -0.0256 meV, still in agreement. One can perform a more advanced calculation, using the experimental charge distribution from [55], as given in Eq. (23). I find $\langle r^3 \rangle = 2.45$ fm^3, significantly lower than Friar and Sick's value. This leads to $R = 0.864$ fm for the exponential model and $R = 0.889$ fm for the Gaussian model, providing shifts of -0.0226 and -0.0232 meV, respectively, in closer agreement to Borie's work. In a recent paper, De Rùjula [17] claimed that the discrepancy found between the charge radii obtained from hydrogen and muonic hydrogen could be due to the fact that theoretical calculations use too simple a dipole model to represent the nucleus. He builds a "toy model" composed of the sum of two dipole functions corresponding to two resonances with different masses. In his model the third moment of the charge distribution is much higher than what is derived from a dipole model, enabling to mostly resolve the discrepancy between the charge radii obtained from muonic and normal hydrogen. He obtained

$$\langle r^3 \rangle_{(2)} = 36.6 \pm 7.3 \approx 43R^3, \tag{49}$$

using R from muonic hydrogen. I use the fit to the experimental form factor from [55] as given in Eq. (23) to check the result from [17] against an experimental determination. I obtain

$$\langle r^3 \rangle_{(2)} \approx 2.4485 \approx 3.98 \times 0.850^3, \tag{50}$$

very close to the dipole model value of Eq. (47). Using the recent MAMI experiment, combined with data from [55], Distler *et al.* [23] obtained

$$\langle r^3 \rangle_{(2)} \approx 2.85(8) \approx 4.18 \times 0.880^3, \tag{51}$$

The conclusions from the authors of [17], which depended on an overly large third moment of the charge distribution, are thus not supported by the experiment.

B. Finite size correction to the Uehling contribution

For the vacuum polarization I obtain, for a point nucleus,

$$\Delta E_{2s_{1/2}-2p_{1/2}}^{11,\text{pn}} = 205.028201 \text{ meV}, \tag{52}$$

to be compared with 205.0282 meV in Ref. [40]. Pachucki [38] obtained 205.0243 meV as the sum of the nonrelativistic 205.0074 meV and first-order relativistic 0.0169 meV corrections. If I calculate the difference between Eq. (52) and the Pachuki nonrelativistic value, I obtain a difference of 0.0208076 meV. This is in excellent agreement with the value provided in Ref. [76], Eq. (6), 0.020843 meV.

To achieve this result I used the mesh parameters described in the previous section, and checked by varying them so that the results were stable within the decimal places provided here. For finite nuclei, I use the same parameters as in the previous section. Again changes in r_0 and h do not change the final value. I obtain

$$\Delta E_{2s_{1/2}-2p_{1/2}}^{11,\text{fs}}(R) = 205.0282076 - 0.02810970909R^2$$
$$+ 0.0007111893365R^3$$
$$- 0.00003572368803R^4. \tag{53}$$

The constant term is in excellent agreement with the one in Eq. (52). This result must be combined to Eq. (45) to obtain values that can be compared with the literature. I obtain

$$\Delta E_{2s_{1/2}-2p_{1/2}}^{11C,\text{fs}}(R) = 205.0282076 - 5.227446248R^2$$
$$+ 0.03529257801R^3$$
$$+ 0.00007356191826R^4$$
$$+ 0.0002788380236R^2\ln(R)$$
$$- 0.00004957597920R^4\ln(R). \tag{54}$$

The R^2 coefficient can be compared to the one in Ref. [76], Table III, which has the value -5.2254 meVfm^{-2}, which contains additional recoil corrections.

For the Uelhing correction to the fine structure, I obtain in the same way

$$\Delta E_{2p_{1/2}-2p_{3/2}}^{11,\text{fs}}(R) = 0.0050157881 - 1.1662334 \times 10^{-7}R^2$$
$$+ 2.2741334 \times 10^{-9}R^3$$
$$- 1.5308196 \times 10^{-10}R^4 \text{ meV}, \tag{55}$$

where the constant term is again in perfect agreement with Borie's value 0.0050 meV [74] (Table 7).

C. Finite size correction to the Källén and Sabry contribution

We can then evaluate the Källén and Sabry contribution $\Delta E_{2p_{1/2}}^{21} - \Delta E_{2s_{1/2}}^{21}$ using V_{21} calculated following Sec. IV, with good accuracy, using our numerical wave functions. For a point nucleus I obtain

$$\Delta E_{2s_{1/2}-2p_{1/2}}^{21,\text{pn}} = 1.508097 \text{ meV}, \tag{56}$$

in agreement with the result of the authors of [38], 1.5079 meV, and in excellent agreement with the one from the authors of [40], 1.5081 meV. Using the wave functions calculated with the proton size, I can also evaluate the finite size correction to the Källén and Sabry contribution. A direct fit to the numerical data gives a result of the form

$$\Delta E_{2s_{1/2}-2p_{1/2}}^{21,\text{fs}}(R) = 1.508097 - 0.00021341293R^2$$
$$+ 7.3404895 \times 10^{-6}R^3$$
$$- 5.0291143 \times 10^{-7}R^4 \text{ meV}, \tag{57}$$

and

$$\Delta E_{2p_{1/2}-2p_{3/2}}^{21,\text{fs}}(R) = 0.0000414300 - 9.25489 \times 10^{-10}R^2$$
$$+ 2.33622 \times 10^{-11}R^3$$
$$- 1.80063 \times 10^{-12}R^4 \text{ meV}, \tag{58}$$

for the fine structure, to be compared with 0.00004 meV in [74].

VI. HIGHER-ORDER VACUUM POLARIZATION CORRECTIONS

A. Higher-order vacuum polarization

The term named "VP iteration," which corresponds to Fig. 7, is given by Eq. (215) of Ref. [39]

$$\Delta E_{\text{VPVP}}(2s) = 0.01244 \frac{4}{9} \left(\frac{\alpha}{\pi} \right)^2 (Z\alpha)^2 \mu_r c^2, \tag{59}$$
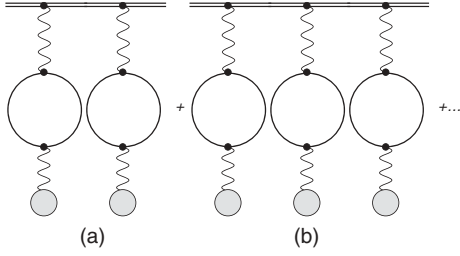
FIG. 7. Feynman diagrams obtained when the Uehling potential is added to the nuclear potential in the Dirac equation. A double line represents a bound electron wave function or propagator and a wavy line a Coulomb photon propagator. The gray circles correspond to the interaction with the nucleus. Diagram (b) corresponds to Fig. 5 and the third term in Eq. (25) in Ref. [77].

where $\mu_r = 94.96446$ MeV for muonic hydrogen (using [11]). This adds 0.15086 meV to the Lamb shift for muonic hydrogen. The Uehling potential under the form used in Sec. III can be introduced in the potential of the Dirac equation (3) when solving it numerically. This amounts to obtaining the exact solution with any number of vacuum polarization insertions as shown in Fig. 7. The numerical methods that we used were described in Refs. [60,61]. Because of the logarithmic dependence of the point nucleus Uehling potential at the origin, I do not calculate the iterated vacuum polarization directly for a point nucleus. I instead calculate for different mean-square radii and charge distribution models, and fit the curves with $f(R) = a + bR^2 + cR^3 + dR^4$. All four models provide very similar values. The final value is

$$\Delta E_{2s_{1/2}-2p_{1/2}}^{11,\text{loop},\text{fs}}(R) = 0.15102161 - 0.000098409804R^2$$
$$+ 7.9038238 \times 10^{-6}R^3$$
$$- 7.2004764 \times 10^{-7}R^4 \,\text{meV}. \qquad (60)$$

The value calculated in Ref. [38] is 0.1509 meV and the one in Ref. [40] is 0.1510 meV, in very good agreement with the present work. The method employed here provides an addition to the proton size dependence for this correction, which was not calculated before. For the fine structure, I obtain in the same way

$$\Delta E_{2p_{1/2}-2p_{3/2}}^{11,\text{loop},\text{fs}}(R) = 2.33197 \times 10^{-6} - 1.77101 \times 10^{-9}R^2$$
$$+ 9.36429 \times 10^{-10}R^3$$
$$- 1.79951 \times 10^{-10}R^4 \,\text{meV}. \qquad (61)$$

B. Other higher-order Uehling corrections

Since we include the vacuum polarization in the Dirac equation potential, all energies calculated by perturbation using the numerical wave function contain the contribution of higher-order diagrams where the external legs, which represent the wave function, can be replaced by a wave function and a bound propagator with one or several vacuum polarization insertions. For example, the Källén and Sabry correction calculated in this way, contains a correction of the type
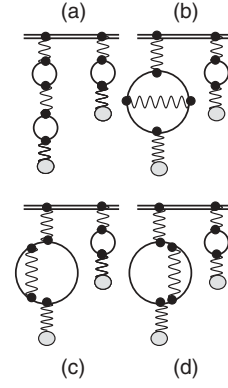

FIG. 8. Lower-order Feynman diagrams included in the Källén and Sabry $V_{21}(r)$ potential, when the Uehling potential is included in the differential equation. See Figs. 4 and 7 for an explanation of symbols. Diagrams (a) and (b) exactly correspond to diagrams (a) and (b) in Fig. 5 and Eq. (25) in Ref. [77].

presented in Fig. 8. This correction is given by

$$\Delta E_{2s_{1/2}-2p_{1/2}}^{21\times11,\text{fs}}(R) = 0.0021552 - 1.32976 \times 10^{-6}R^2$$
$$+ 9.4577 \times 10^{-8}R^3$$
$$- 8.5185 \times 10^{-9}R^4 \,\text{meV}, \qquad (62)$$

with a 10^{-7} meV accuracy. This correction is part of the three-loop corrections from [77,78]. The diagrams in Fig. 8 correspond to Figs. 5(a) and 5(b) in Ref. [77] and Figs. 2(e) (upper left) and 2(f) of Ref. [79]. The sum of the contributions of the diagrams Fig. 8(a) and 8(b) is 0.00223, in good agreement with our all-order fully relativistic result. The three-loop diagram Fig. 5(c) of Ref. [77] and Fig. 2(g) of Ref. [79] is included in the all-order contribution obtained by solving numerically the Dirac equation with the Uëlhing potential. For the fine structure this correction is very small

$$\Delta E_{2p_{1/2}-2p_{3/2}}^{21\times11,\text{fs}}(R) = 3.75754 \times 10^{-8} - 3.49318 \times 10^{-12}R^2$$
$$+ 2.58244 \times 10^{-13}R^3$$
$$- 2.74201 \times 10^{-14}R^4 \,\text{meV}. \qquad (63)$$

C. Wichmann and Kroll correction

We use the approximate potentials as presented in Refs. [72, 80] to evaluate the Wichmann and Kroll [81] V_{13} correction to the Uehling potential. The corresponding diagram is shown in Fig. 4(b). This contribution is given together with the light-by-light scattering diagrams of Fig. 9 in Refs. [77,79,82]. We find for a point nucleus, the exact value, and a size correction, given by

$$\Delta E_{2s_{1/2}-2p_{1/2}}^{13,\text{fs}}(R) = -0.0010170628 + 5.5414179 \times 10^{-8}R^2$$
$$- 5.1356872 \times 10^{-10}R^3$$
$$- 1.9364450 \times 10^{-11}R^4 \,\text{meV}, \qquad (64)$$

to be compared to the value given in Ref. [79] (Table III) of $-0.001018(4)$ meV. In the lowest-order approximation, the diagram in Fig. 9(a) provides an energy shift of $\Delta E_{13}/Z^2$ [79,82]. For the fine structure, this correction is comparable to
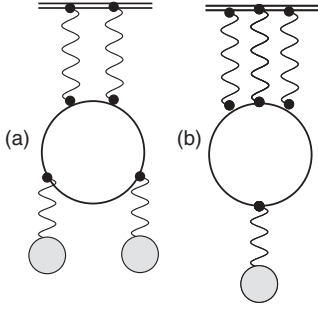
FIG. 9. Feynman diagrams for the light-by-light scattering. See Figs. 4 and 7 for an explanation of symbols.

the contribution from Eq. (63)

$$\Delta E_{2p_{1/2}-2p_{3/2}}^{13,\text{fs}}(R) = -4.21088 \times 10^{-8} + 4.41081 \times 10^{-13}R^2$$
$$-8.49036 \times 10^{-15}R^3$$
$$+1.81474 \times 10^{-15}R^4 \text{ meV}. \quad (65)$$

D. Muon radiative corrections

1. Muon self-energy

Highly accurate self-energy values for electronic atoms and point nucleus are known from [83]. The self-energy correction, represented in Fig. 10, is conveniently expressed by the slowly varying function $F(Z\alpha)$ defined by

$$\Delta E_{SE} = \frac{\alpha}{\pi} \frac{(Z\alpha)^4}{n^3} mc^2 F(Z\alpha), \quad (66)$$

where m is the particle mass.

The recoil corrections to $F(Z\alpha)$ are described in detail in Ref. [11]. The dependence in the reduced mass has to be included leading to the following expressions, specialized for the $n = 2$ shells:

$$\Delta E_{\mu SE,2S} = \frac{\alpha}{\pi} \frac{(Z\alpha)^4}{8} \left(\frac{\mu_r}{m_\mu}\right)^3 m_\mu c^2 \left\{ -\frac{4}{3} \ln k_0(2S) + \frac{10}{9} \right.$$
$$+ \frac{4}{3} \ln\left(\frac{m_\mu}{\alpha^2 \mu_r}\right) + \left(\frac{139}{32} - 2\ln 2\right)\pi\alpha$$
$$+ \left(\frac{67}{30} + \frac{16\ln 2}{3}\right) \ln\left(\frac{m_\mu}{\alpha^2 \mu_r}\right)\alpha^2$$
$$\left. - \left[\ln\left(\frac{m_\mu}{\alpha^2 \mu_r}\right)\right]^2 \alpha^2 \alpha^2 G_{2s}(\alpha) \right\}, \quad (67)$$

$$\Delta E_{\mu SE,2p_{1/2}} = \frac{\alpha}{\pi} \frac{(Z\alpha)^4}{8} \left(\frac{\mu_r}{m_\mu}\right)^3 m_\mu \left[-\frac{4}{3} \ln k_0(2P) \right.$$
$$- \frac{1}{6}\left(\frac{m_\mu}{\mu_r}\right) + \frac{103}{180} \ln\left(\frac{m_\mu}{\alpha^2 \mu_r}\right)\alpha^2$$
$$\left. + \alpha^2 G_{2p_{1/2}}(\alpha) \right], \quad (68)$$

FIG. 10. Feynman diagrams for the muon self-energy. See Figs. 4 and 7 for explanation of symbols.

and

$$\Delta E_{\mu SE,2p_{3/2}} = \frac{\alpha}{\pi} \frac{(Z\alpha)^4}{8} \left(\frac{\mu_r}{m_\mu}\right)^3 m_\mu \left[-\frac{4}{3} \ln k_0(2P) \right.$$
$$+ \frac{1}{12}\left(\frac{m_\mu}{\mu_r}\right) + \frac{29}{90} \ln\left(\frac{m_\mu}{\alpha^2 \mu_r}\right)\alpha^2$$
$$\left. + \alpha^2 G_{2p_{3/2}}(\alpha) \right]. \quad (69)$$

The Bethe logarithms are given by $\ln k_0(2S) = 2.811769893$ and $\ln k_0(2P) = -0.030016709$ [84]. The remainders are given by $G_{2s}(\alpha) = -31.185150(90)$, $G_{2p_{1/2}}(\alpha) = -0.97350(20)$, and $G_{2p_{3/2}}(\alpha) = -0.48650(20)$ [83,85]. One then gets the exact muon self-energy for each state. For the $2s$ state, this gives 0.675150 meV instead of 0.675389 meV. For the $2p_{1/2}$ I get -0.00916882 meV and for $2p_{3/2}$, 0.008393377 meV in place of 0.01424054 and -0.00332838 meV, respectively, if one would use only the low-order A_{40} term.

The finite size correction is given by perturbation theory [11] Eq. (54)

$$E_{SE-NS}(R,Z\alpha) = \left(4\ln 2 - \frac{23}{4}\right)\alpha(Z\alpha)\mathcal{E}_{NS}(R,Z\alpha), \quad (70)$$

where ([11] Eq. (51))

$$\mathcal{E}_{NS}(R,Z\alpha) = \frac{2}{3}\left(\frac{\mu_r}{m_\mu}\right)^3 \frac{(Z\alpha)^2}{n^3} m_\mu \left(\frac{Z\alpha R}{\lambda_C}\right)^2, \quad (71)$$

is the lowest-order finite nuclear size correction to the Coulomb energy. Here $\lambda_C = 1.867594282$ fm is the muon Compton wavelength. Equation (71) provides $\mathcal{E}_{NS}(R) = 5.19745R^2$ for muonic hydrogen in agreement with [38,40].

The self-energy correction to the Lamb shift with finite size correction is then

$$\Delta E_{2p_{1/2}}^{SE,\text{fs}} - \Delta E_{2s_{1/2}}^{SE,\text{fs}}(R)$$
$$= -0.68431882 + 0.000824062R^2 \text{ meV}, \quad (72)$$

and to the fine structure:

$$\Delta E_{2p_{3/2}}^{SE,\text{fs}} - \Delta E_{2p_{1/2}}^{SE,\text{fs}} = 0.017562197 \text{ meV}. \quad (73)$$

It should be noted that in Ref. [40], the R^2-dependent part of the $2s$ self-energy is much larger than what is given in Eq. (72). This value was checked independently by using an all-order calculation with finite size, following the work of Mohr and Soff [86]. The results of this calculation agrees well with Eq. (72) and is given by [87]

$$E_{SE-NS}^H(Z=1,R) = -0.68431882 + 0.00082432235R^2$$
$$-0.000014586790R^3$$
$$+1.2893445 \times 10^{-6}R^4$$
$$-5.5355294 \times 10^{-8}R^5 \text{ meV}. \quad (74)$$

2. Muon loop vacuum polarization

The vacuum polarization due to the creation of virtual muon pairs is represented by the same Feynman diagram as in Fig. 4(a) and same equations (28) as vacuum polarization due to electron-positron pairs, replacing the electron Compton

wavelength by the muon one. For S states, it is given by [11] Eq. (27), [36] Eq. (32)

$$E_{\mu VP}(ns) = -\frac{\alpha(\alpha Z)^4}{\pi n^3}\left(-\frac{4}{15} + \pi\alpha\frac{5}{48}\right)\left(\frac{\mu_r}{m_\mu}\right)^3 m_\mu c^2, \quad (75)$$

in which higher-order terms in $Z\alpha$ have been neglected. For the $2s$ Lamb shift in muonic hydrogen it gives 0.01669 meV and is included in Refs. [38,40,88] Eq. (2.29) for the first α correction. As it is a sizable contribution, and the muon Compton wavelength, which represent the scale of QED corrections for muons is of the order of the finite nuclear size (1.9 fm), one could expect a nonnegligible finite size contribution. Using the numerical procedure described in Sec. III, replacing the electron Compton wavelength by the muon one in Eq. (28), I obtain

$$\Delta E_{2s_{1/2}-2p_{1/2}}^{\mu 11,\text{fs}}(R) = 0.01671487464 - 0.00005279721702R^2$$
$$+ 0.00001269866912R^3$$
$$- 5.360546098 \times 10^{-6}R^4$$
$$+ 0.00001717649157R^2\ln(R)$$
$$+ 2.047113814 \times 10^{-6}R^4\ln(R)\,\text{meV}, \quad (76)$$

where the constant term is in excellent agreement with Eq. (75) and the R dependence explicit. From [11], Eq. (55), one obtains

$$E_{\mu VP}^{\text{fs}}(ns) = \tfrac{3}{4}\alpha(Z\alpha)\mathcal{E}_{NS}(R,\alpha) = 0.00020758R^2\,\text{meV} \quad (77)$$

for the $2s$ level. This term is about four times larger than the numerical coefficient for R^2 in Eq. (76).

Using the wave function evaluated with the Uehling potential in the Dirac equation, I also obtain the value of the sum of the diagrams with one muon vacuum polarization loop and any number of electron loops on each side, as in Fig. 7, with one loop being a muon loop

$$\Delta E_{2s_{1/2}-2p_{1/2}}^{\mu 11\times 11,\text{fs}}(R) = 0.00005348857 - 5.358667885 \times 10^{-7}R^2$$
$$+ 6.495888541 \times 10^{-8}R^3$$
$$- 4.287455607 \times 10^{-8}R^4$$
$$+ 2.822488184 \times 10^{-7}R^2\ln(R)$$
$$+ 1.739448734 \times 10^{-8}R^4\ln(R)\,\text{meV}. \quad (78)$$

This muonic vacuum polarization is a small contribution to the fine structure

$$\Delta E_{2p_{1/2}-2p_{3/2}}^{\mu 11\times 11,\text{fs}}(R) = 1.67794 \times 10^{-7} - 2.10861 \times 10^{-10}R^2$$
$$+ 8.51427 \times 10^{-11}R^3$$
$$- 1.38884 \times 10^{-11}R^4\,\text{meV}. \quad (79)$$

VII. EVALUATION OF THE RECOIL CORRECTIONS

The relativistic treatment of recoil corrections is described in, e.g., [11], Eq. (10). The analytic solution of the Dirac equation for a point nucleus and a particle of mass m is given by

$$E_D = mc^2 f(n,j) \quad (80)$$

with

$$f(n,j) = \frac{1}{\sqrt{1 + \frac{(Z\alpha)^2}{\left(n-j+\frac{1}{2}+\sqrt{(j+\frac{1}{2})^2-(Z\alpha)^2}\right)^2}}}. \quad (81)$$

The recoil can then be included by evaluating [66,89]

$$E_M = Mc^2 + \mu_r c^2[f(n,j) - 1] + \frac{[f(n,j)-1]^2\,\mu_r^2 c^2}{2M} \quad (82)$$

$$+ \frac{1-\delta_{l,0}}{\kappa(2l+1)}\frac{(Z\alpha)^4\mu_r^3 c^2}{2n^3 M_p^2}, \quad (83)$$

where $M = m_\mu + M_p$. If one expands the previous equation in powers of $(Z\alpha)$, one would find that the terms of order up to $(Z\alpha)^4$ are identical to what is given in Ref. [66]. We also compared the numerical results from our numerical approach for the point nucleus, as described in Sec. II A to what can be obtained by using directly (80) and find excellent agreement. Below, we will make exclusive use of the direct numerical evaluation of the Dirac equation. The relativistic corrections to Eq. (83) associated with the motion of the nucleus are called relativistic-recoil correction. The correction to order $(Z\alpha)^5$ and to all orders in m_μ/M_p is given by [11,42,89,90]

$$E_{RR}^5(n,l) = \frac{\mu_r^3 c^2}{m_\mu M_p}\frac{(Z\alpha)^5}{\pi n^3}\left\{\frac{\delta_{l,0}}{3}\ln\frac{1}{(Z\alpha)^2} - \frac{8}{3}\ln k_0(l,n)\right.$$
$$- \frac{\delta_{l,0}}{9} - \frac{7}{3}a_{n,l} - \frac{2\delta_{l,0}}{M_p^2 - m_\mu^2}$$
$$\left.\times\left[M_p^2\ln\left(\frac{m_\mu}{\mu_r}\right) - m_\mu^2\ln\left(\frac{M_p}{\mu_r}\right)\right]\right\}, \quad (84)$$

where

$$a_{n,l} = -2\left[\ln\left(\frac{2}{n} + \sum_{i=1}^{n}\frac{1}{i}\right) + 1 - \frac{1}{2n}\right]\delta_{l,0}$$
$$+ \frac{1-\delta_{l,0}}{l(l+1)(2l+1)}. \quad (85)$$

This correction corresponds to the diagrams in Fig. 11.

The next order of the relativistic recoil corrections is given for s states by

$$E_{RR}^6(ns) = \frac{m_\mu}{M_p}\frac{(Z\alpha)^6}{n^3}m_\mu c^2\left\{4\ln 2 - \frac{7}{2} - \frac{11}{60\pi}\ln\frac{1}{(Z\alpha)^2}\right\}, \quad (86)$$
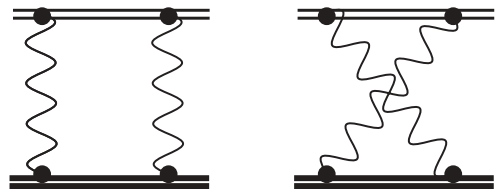

FIG. 11. Feynman diagrams corresponding to the relativistic recoil correction (84). The heavy double line represents the proton wave function or propagator. The other symbols are explained in Fig. 4.

and for $l \geqslant 1$ states by

$$
E_{\mathrm{RR}}^6(nl) = \frac{m_\mu}{M_p} \frac{(Z\alpha)^6}{n^3} m_\mu c^2 \left\{ \left[3 - \frac{l(l+1)}{n^2} \right] \right.
$$
$$
\left. \times \frac{2}{(4l^2 - 1)(2l + 3)} \right\}. \tag{87}
$$

Using Eqs. (82) to (87), I obtain

$$
\Delta E_{2s_{1/2}-2p_{1/2}}^{\mathrm{Rec.}} = 0 + 0.0574706 - 0.0449705
$$
$$
= 0.0125001 \, \text{meV}, \tag{88}
$$

and to the fine structure

$$
\Delta E_{2p_{1/2}-2p_{3/2}}^{\mathrm{Rec.}} = 0.0000051 - 0.0862059 + 0
$$
$$
= -0.0862008 \, \text{meV}. \tag{89}
$$

This is in excellent agreement with the results from the authors of [74].

VIII. EVALUATION OF SOME ALL-ORDER HYPERFINE STRUCTURE CORRECTIONS

The expression of the hyperfine magnetic dipole operator can be written as

$$
H_{\mathrm{hfs}} = -ec\boldsymbol{\alpha} \cdot \boldsymbol{A}(r) = -ec\boldsymbol{\alpha} \cdot \boldsymbol{A}(r), \tag{90}
$$

with

$$
\boldsymbol{A}(r) = \frac{\mu_0}{4\pi} \frac{\boldsymbol{\mu} \times \boldsymbol{r}}{r^3}, \tag{91}
$$

where $\boldsymbol{\mu}$ is the nuclear magnetic moment and we have assumed a magnetic moment distribution of a point particle for the nucleus. It is convenient to express H_{hfs} using vector spherical harmonics. On obtains [91–94]

$$
H_{\mathrm{hfs}} = \boldsymbol{M}^1 \cdot \boldsymbol{T}^1, \tag{92}
$$

where

$$
\boldsymbol{T}^1(r) = -ie\sqrt{\frac{8\pi}{3}} \frac{\boldsymbol{\alpha} \cdot \boldsymbol{Y}_{1q}^{(0)}(\hat{r})}{r^2}, \tag{93}
$$

and $\boldsymbol{M}^1$ represents the magnetic moment operator from the nucleus. The operator $\boldsymbol{T}^1$ acts only on the bound particle coordinates. The vector spherical harmonic $\boldsymbol{Y}_{1q}^{(0)}(\hat{r})$ is an eigenfunction of $\boldsymbol{J}^2$ and J_z, defined as [92,94–97]

$$
\boldsymbol{Y}_{1q}^{(0)}(\hat{r}) = \boldsymbol{Y}_{11q}(\hat{r})
$$
$$
= \sum_\sigma C(1,1,1; q-\sigma, \sigma, q) Y_{1,q-\sigma}(\hat{r}) \boldsymbol{\xi}_\sigma, \tag{94}
$$

where $C(j_1, j_2, j; m_1, m_2, m)$ is a Clebsh-Gordan coefficient, $Y_{1,q}$ are scalar spherical harmonic, and $\boldsymbol{\xi}_\sigma$ are eigenvectors of s^2 and s_z, the spin-one matrices [92,94–97]. The reduction to radial and angular integrals is presented in various works [92–94]. In heavy atoms, the hyperfine structure correction due to the magnetic moment contribution is usually calculated for a finite charge distribution, but a point magnetic dipole moment (see, e.g., [92,93]). When matrix elements nondiagonal in J are needed, one can use [98] for a one-particle atom

$$
\Delta E_{\mathrm{M1}}^{\mathrm{hfs}} = A \frac{g\alpha}{2M_p} \int_0^\infty dr \frac{P_1(r)Q_2(r) + P_2(r)Q_1(r)}{r^2}, \tag{95}
$$

where $g = \mu_p/2 = 2.792847356$ for the proton, is the anomalous magnetic moment, A is an angular coefficient

$$
A = (-1)^{I+j_1+F} \frac{\left\{ \begin{smallmatrix} I & j_1 & F \\ j_2 & I & k \end{smallmatrix} \right\}}{\left(\begin{smallmatrix} I & 1 & I \\ -I & 0 & I \end{smallmatrix} \right)} (-1)^{J_1 - \frac{1}{2}} \sqrt{(2J_1+1)(2J_2+1)}
$$
$$
\times \begin{pmatrix} j_1 & 1 & j_2 \\ \frac{1}{2} & 0 & -\frac{1}{2} \end{pmatrix} \pi(l_1, k, l_2), \tag{96}
$$

where $\pi(l_1, k, l_2) = 0$ if $l_1 + l_2 + 1$ is odd and 1 otherwise. The j_i are the total angular momentum of the i state for the bound particle, l_i are orbital angular momentum, I is the nuclear spin, k the multipole order [$k = 1$ for the magnetic dipole contribution described in Eq. (95)], and F the total angular momentum of the atom. The difference between ΔE^{hfs} values calculated with a finite or point nuclear charge contribution is called the Breit-Rosenthal correction [99].

To consider a finite magnetic moment distribution, one uses the Bohr-Weisskopf correction [100]. The correction can be written [101]

$$
\Delta E^{\mathrm{BW}} = -A \frac{g\alpha}{2M_p} \int_0^\infty dr_n r_n^2 \mu(r_n)
$$
$$
\times \int_0^{r_n} dr \frac{P_1(r)Q_2(r) + P_2(r)Q_1(r)}{r^2}, \tag{97}
$$

where the magnetic moment density $\mu(r_n)$ is normalized as

$$
\int_0^\infty dr_n r_n^2 \mu(r_n) = 1. \tag{98}
$$

Borie and Rinker [102] wrote the total diagonal hyperfine energy correction for a muonic atom as

$$
\Delta E_{i,j} = \frac{4\pi\kappa[F(F+1) - I(I+1) - j(j+1)]}{\kappa^2 - \frac{1}{4}} \frac{g\alpha}{2M_p}
$$
$$
\times \int_0^\infty dr \frac{P_1(r)Q_2(r)}{r^2} \int_0^r dr_n r_n^2 \mu_{\mathrm{BR}}(r_n), \tag{99}
$$

where the normalization is different

$$
\int_0^\infty d^3 r_n \mu_{\mathrm{BR}}(r_n) = 4\pi \int_0^\infty dr_n r_n^2 \mu_{\mathrm{BR}}(r_n) = 1. \tag{100}
$$

This means that $\mu_{\mathrm{BR}}(r) = \mu(r)/(4\pi)$. The evaluation of the Wigner $3j$ and $6j$ symbols in Eq. (96) give the same angular factor as in Eq. (95).

The equivalence of the two formalisms can be easily checked: Starting from Eq. (99) and dropping the angular factors, we get, doing an integration by parts

$$
\int_0^\infty dr \frac{P_1(r)Q_2(r)}{r^2} \int_0^r dr_n r_n^2 \mu(r_n)
$$
$$
= \left[\int_0^r dr_n r_n^2 \mu(r_n) \int_0^r dt \frac{P_1(t)Q_2(t)}{t^2} \right]_0^\infty
$$
$$
- \int_0^\infty dr_n r_n^2 \mu(r_n) \int_0^{r_n} dr \frac{P_1(r)Q_2(r)}{r^2}
$$
$$
= \int_0^\infty dr \frac{P_1(r)Q_2(r)}{r^2}
$$
$$
- \int_0^\infty dr_n r_n^2 \mu(r_n) \int_0^{r_n} dr \frac{P_1(r)Q_2(r)}{r^2}, \tag{101}
$$

where we have used Eq. (98). We thus find that the formula in Borie and Rinker represents the *full* hyperfine structure (HFS) correction, including the Bohr-Weisskopf part.

In 1956, Zemach [103] calculated the hyperfine structure energy of hydrogen, including the recoil effects. He showed that in first order in the finite size, the HFS depends on the charge *and* magnetic distribution moments only through the Zemach's form factor defined in Eq. (15). The proton is assumed to be at the origin of coordinates. Its charge and magnetic moment distribution are given in terms of charge distribution $\rho(r)$ and magnetic moment distributions $\mu(r)$. Zemach calculated the correction in first order to the hyperfine energy of s states of hydrogen due to the electric charge distribution. The HFS energy is written as

$$\Delta E^Z_{\mathrm{hfs}} = -\frac{2}{3}\langle \boldsymbol{S}_p \cdot \boldsymbol{S}_\mu \rangle \int |\phi(\boldsymbol{r})|^2 \mu(\boldsymbol{r}) d\boldsymbol{r} \qquad (102)$$

where ϕ is the nonrelativistic electron wave function and S_x are the spin operators of the electron and proton. If the magnetic moment distribution is taken to be the one of a point charge $\mu(\boldsymbol{r}) = \delta(\boldsymbol{r})$, the integral reduces to $|\phi(0)|^2$. The first-order correction to the wave function due to the nucleus finite charge distribution is given by

$$\phi(\boldsymbol{r}) = \phi_{\mathrm{C}}(0)\left(1 - \alpha m_\mu \int \rho(\boldsymbol{u})|\boldsymbol{u} - \boldsymbol{r}|d\boldsymbol{u}\right), \qquad (103)$$

where $\phi_{\mathrm{C}}(0)$ is the unperturbed Coulomb wave function at the origin for a point nucleus. Replacing into Eq. (102) and keeping only first order terms, we get [Eq. (2.8) of [103] corrected for a misprint]

$$\Delta E^Z_{\mathrm{hfs}} = -\frac{2}{3}\langle \boldsymbol{S}_p \cdot \boldsymbol{S}_\mu \rangle |\phi_{\mathrm{C}}(0)|^2$$
$$\times \left(1 - 2\alpha m_\mu \int \rho(\boldsymbol{u})|\boldsymbol{u} - \boldsymbol{r}|\mu(\boldsymbol{r})d\boldsymbol{u}d\boldsymbol{r}\right),$$
$$= E_{\mathrm{F}}\left(1 - 2\alpha m_\mu \int \rho(\boldsymbol{u})|\boldsymbol{u} - \boldsymbol{r}|\mu(\boldsymbol{r})d\boldsymbol{u}d\boldsymbol{r}\right), \qquad (104)$$

where E_F is the well known HFS Fermi energy. Transforming Eq. (104) using $\boldsymbol{r} \to \boldsymbol{r} + \boldsymbol{u}$, and so on Zemach obtained

$$\Delta E^Z_{\mathrm{hfs}} = E_{\mathrm{F}}(1 - 2\alpha m_\mu \langle r_{\mathbf{Z}} \rangle), \qquad (105)$$

with $\langle r_{\mathbf{Z}} \rangle$ given in Eq. (16). The $2s$-state Fermi energy is given by

$$E^{2s}_{\mathrm{F}} = \frac{(Z\alpha)^4}{3} g_p \frac{\mu_r^3}{m_p m_\mu}. \qquad (106)$$

A. Hyperfine structure of the 2s level

To check the dependence of the hyperfine structure on the Zemach radius and on the proton finite size, I have performed a series of calculations for a dipolar distribution for both the charge and magnetic moment distribution. We can then study the dependence of the HFS beyond the first order corresponding to the Zemach correction. I calculated the hyperfine energy splitting $\Delta E_{\mathrm{hfs}}(R_{\mathrm{Z}}, R) = E_{\mathrm{hfs}}(R) + E^{\mathrm{BW}}_{\mathrm{hfs}}(R, R_M)$ numerically. I also evaluate with and without the self-consistent inclusion of the Uëhling potential in the calculation, to obtain

an all-order Uëhling contribution to the HFS energy. We calculated the correction $\Delta E_{\mathrm{hfs}}(R_{\mathrm{Z}}, R)$ for several values of R_{Z} between 0.8 and 1.15 fm, and proton sizes ranging from 0.3 to 1.2 fm, by steps of 0.05 fm, which represents 285 values. The results show that the correction to the HFS energy due to charge and magnetic moment distribution is not quite independent of R as one would expect from Eq. (105), in which the finite size contribution depends *only* on R_{Z}. We fitted the hyperfine structure splitting of the $2s$ level, $E^{2s}_{\mathrm{hfs}}(R_{\mathrm{Z}}, R)$ by a function of R and R_{Z}, which gives

$$E^{2s}_{\mathrm{hfs}}(R_{\mathrm{Z}}, R)$$
$$= 22.807995 - 0.0022324349R^2$$
$$\quad + 0.00072910794R^3 - 0.000065912957R^4$$
$$\quad - 0.16034434R_{\mathrm{Z}} - 0.00057179529RR_{\mathrm{Z}}$$
$$\quad - 0.00069518048R^2R_{\mathrm{Z}} - 0.00018463878R^3R_{\mathrm{Z}}$$
$$\quad + 0.0010566454R^2_{\mathrm{Z}} + 0.00096830453RR^2_{\mathrm{Z}}$$
$$\quad + 0.00037883473R^2R^2_{\mathrm{Z}} - 0.00048210961R^3_{\mathrm{Z}}$$
$$\quad - 0.00041573690RR^3_{\mathrm{Z}} + 0.00018238754R^4_{\mathrm{Z}} \text{ meV}.$$
$$(107)$$

The constant term should be close to the sum of the Fermi energy 22.80541 meV and of the Breit term [104] the HFS correction calculated with a point-nucleus Dirac wave function for which I find 22.807995 meV. When setting the speed of light to infinity in the program I recover exactly the Fermi energy. The Breit contribution is thus 0.002595 meV, to be compared to 0.0026 meV in Ref. [41] (Table II, line 3) and 0.00258 meV in Ref. [74]. Martynenko [41] evaluated this correction, which he named "Proton structure corrections of order α^5 and α^6," to be -0.1535 meV, following [36]. He finds the coefficient for the Zemach's radius to be -0.16018 meVfm^{-1}, in very good agreement with the present all-order calculation -0.16034 meVfm^{-1}. Borie's value [74] -0.16037 meVfm^{-1} is even closer. The difference between Borie's value and Eq. (107) is represented in Fig. 12 as a function of the charge and Zemach radii. The maximum difference is around 1 μeV.

In Ref. [36], the charge and magnetic moment distributions are written down in the dipole form, which corresponds to Eq. (13)

$$G_E(q^2) = \frac{G_M(q^2)}{1 + \kappa_p} = \frac{\Lambda^4}{(\Lambda^2 + q^2)^2}, \qquad (108)$$

with $\Lambda = 848.5$ MeV. This leads to $R = 0.806$ fm as in Ref. [2] and $R_{\mathrm{Z}} = 1.017$ fm using this definition for the form factor in Eq. (17). Moreover there are recoil corrections included. Pachucki [36] found that the pure Zemach contribution (in the limit $m_p \to \infty$) is -0.183 meV. In Ref. [105], the Zemach corrections were given as δ (Zemach) $\times E_F = -71.80 \times 10^{-4} E_F$, for $R_{\mathrm{Z}} = 1.022$ fm. This leads to a coefficient -0.1602 meVfm^{-1}, in excellent agreement with our value -0.16036 meVfm^{-1}.

The effect of the vacuum polarization on the $2s$ hyperfine structure energy shift as a function of the Zemach and charge radius have been calculated for the same set of values as the main contribution. The data can be described as a function of
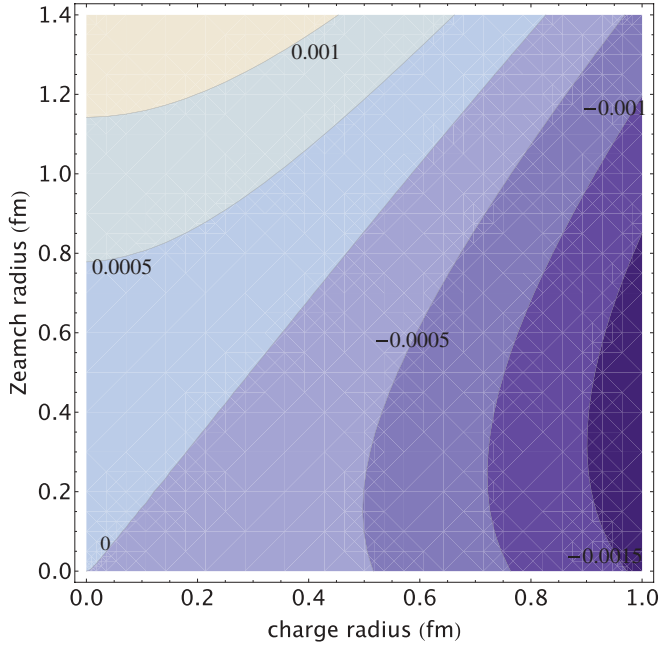
FIG. 12. (Color online) Difference between Borie's value and Eq. (107) result as a function of the charge and Zemach radii (meV).

R_Z and R as

$$E_{\mathrm{hfs}}^{2s,\mathrm{VP}}(R_Z, R)$$
$$= 0.074369030 + 0.000074236132 R^2$$
$$+ 0.00013277334 R^3 - 8.0987285 \times 10^{-6} R^4$$
$$- 0.0017880269 R_Z - 0.00017204505 R R_Z$$
$$- 0.00037499458 R^2 R_Z - 0.000070355379 R^3 R_Z$$
$$- 0.00022093411 R_Z^2 + 0.00035038656 R R_Z^2$$
$$+ 0.00020554316 R^2 R_Z^2 + 0.00025100642 R_Z^3$$
$$- 0.00017200435 R R_Z^3 - 0.000061266973 R_Z^4 \text{ meV}.$$
$$\tag{109}$$

It corresponds to the diagrams presented in Fig. 13. The size-independent term 0.07437 meV corresponds to the sum of the two contributions represented by the two top diagrams in Fig. 13 and is given as $\Delta \mathrm{E}_{\mathrm{1loop\text{-}after\text{-}loop VP}}^{\mathrm{hfs}} = 0.0746$ meV in Ref. [41]. The term $\Delta E_{1\gamma,\mathrm{VP}}^{\mathrm{hfs}} = 0.0481$ meV corresponds to a vacuum polarization loop in the HFS potential [36,41, 102], which is not evaluated here. The corrections present in Ref. [74] not included in Eqs. (107) and (109) give an extra contribution of

$$E_{\mathrm{hfs}}^{2s,\mathrm{HO}} = 0.10287 \text{ meV}. \tag{110}$$

Combining Eqs. (107), (109), and (110), I get

$$E_{\mathrm{hfs}}^{2s}(R_Z, R)$$
$$= 22.985234 - 0.0021581988 R^2$$
$$+ 0.00086188128 R^3 - 0.000074011685 R^4$$
$$- 0.16213237 R_Z - 0.00074384033 R R_Z$$
$$- 0.0010701751 R^2 R_Z - 0.00025499415 R^3 R_Z$$
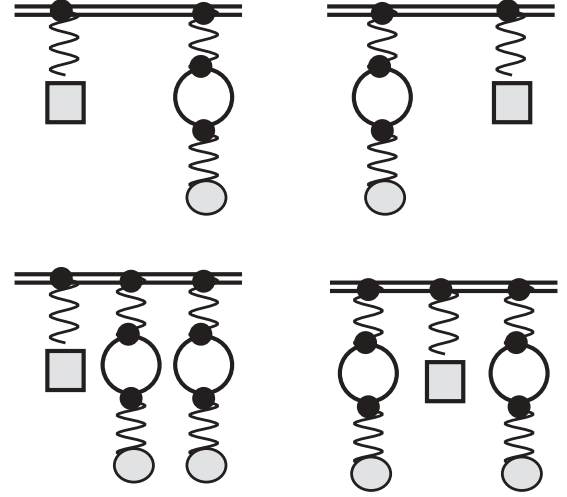$$+ 0.00083571133 R_Z^2 + 0.0013186911 R R_Z^2$$

FIG. 13. Feynman diagrams corresponding to the evaluation of the hyperfine structure using wave functions obtained with the Uehling potential in the Dirac equation. The gray squares correspond to the hyperfine interaction.

$$+ 0.00058437789 R^2 R_Z^2 - 0.00023110319 R_Z^3$$
$$- 0.00058774125 R R_Z^3 + 0.00012112057 R_Z^4 \text{ meV}.$$
$$\tag{111}$$

In Ref. [41], the equivalent expression is

$$E_{\mathrm{hfs}}^{2s\mathrm{Mart.}}(R_Z) = 22.9857 - 0.16018 R_Z \text{ meV}, \tag{112}$$

while it is

$$E_{\mathrm{hfs}}^{2s\mathrm{Borie}}(R_Z) = 22.9627 - 0.16037 R_Z \text{ meV}, \tag{113}$$

in Ref. [74]. Using a Zemach's radius of 0.9477 fm in Eq. (112), needed to reproduce entry 11 in Table II of Ref. [41], one obtains 22.8148 meV as expected. In Eq. (113), it gives 22.8107 meV. Using the same Zemach radius and Eq. (111) I obtain 22.8104 meV with the muonic hydrogen proton radius value and 22.8103 meV with the CODATA one, in excellent agreement with Borie's value. All three values are in agreement with the result 22.8146(49) meV in Ref. [20]. In a recent work, however, the use of form factors in the Breit equations leads to smaller finite size corrections, leading to 22.8560 meV [106]. A comparison between some of these results is presented in Table I.

IX. EVALUATION OF MUONIC HYDROGEN $n = 2$ TRANSITIONS

A. Lamb shift and fine structure

The results presented in this work for the Lamb shift [Eqs. (45), (54), (57), (60), (62), (64), (72), (76), and (78)] can be summarized in the following proton-size-dependent equation:

$$\Delta E_{2s_{1/2}-2p_{1/2}}^{\mathrm{Tot,fs}}(R)$$
$$= 206.0209137 - 5.226988356 R^2 + 0.03530609322 R^3$$
$$+ 0.00006821634516 R^4 - 5.535529372 \times 10^{-8} R^5$$

TABLE I. Comparison of contributions to the 2s hyperfine structure from [41,74] and the present work (meV) for $R_Z = 1.0668$ fm [2] as used in Ref. [41]. Note that in this reference, the proton structure correction of order α^5 (item # 6) may combine the Zemach correction and the recoil correction (# 24). VP: Vacuum polarization.

	#	Ref. [41]	Ref. [74]	This work
Fermi energy	1	22.8054	22.8054	
Dirac energy (includes Breit corr.)	2			22.807995
Vacuum polarization corrections of orders α^5, α^6 in second order perturbation theory ϵ_{VP1}	3	0.0746	0.07443	
All-order VP contribution to HFS, with finite magnetization distribution	4			0.07244
Finite extent of magnetisation density correction to the above	5		−0.00114	
Proton structure corr. of order α^5	6	−0.1518	−0.17108	−0.17173
Proton structure corrections of order α^6	7	−0.0017		
Electron vacuum polarization contribution + proton structure corrections of order α^6	8	−0.0026		
Contribution of 1γ interaction of order α^6	9	0.0003	0.00037	0.00037
$\epsilon_{VP}2E_F$ (neglected in Ref. [41])	10		0.00056	0.00056
Muon loop VP (part corresponding to ϵ_{VP2} neglected in Ref. [41])	11		0.00091	0.00091
Hadronic Vac. Pol.	12	0.0005	0.0006	0.0006
Vertex (order α^5)	13		−0.00311	−0.00311
Vertex (order α^6) (only part with powers of $\ln(\alpha)$, see [107])	14		−0.00017	−0.00017
Breit	15	0.0026	0.00258	
Muon anomalous magnetic moment correction of order α^5, α^6	16	0.0266	0.02659	0.02659
Relativistic and radiative recoil corrections with proton anomalous magnetic moment of order α^6	17	0.0018		
One-loop electron vacuum polarization contribution of 1γ interaction of orders α^5, α^6 (ϵ_{VP2})	18	0.0482	0.04818	0.04818
Finite extent of magnetization density correction to the above	19		−0.00114	−0.00114
One-loop muon vacuum polarization contribution of 1γ interaction of order α^6	20	0.0004	0.00037	0.00037
Muon self energy + proton structure correction of order α^6	21	0.001		0.001
Vertex corrections + proton structure corrections of order α^6	22	−0.0018		−0.0018
"Jellyfish" diagram correction + proton structure corrections of order α^6	23	0.0005		0.0005
Recoil correction [108]	24		0.02123	0.02123
Proton polarizability contribution of order α^5	25	0.0105		
Proton polarizability [108]	26		0.00801	0.00801
Weak interaction contribution	27	0.0003	0.00027	0.00027
Total		22.8148	22.8129	22.8111

$$+ 0.0002962967640 R^2 \ln(R)$$
$$- 0.00004751147090 R^4 \ln(R) \text{ meV}. \tag{114}$$

In the same way, Eqs. (46), (55), (58), (61), (63), (65), (73), (79), and (89) lead to the fine structure interval [which include the recoil corrections (89), included in Table II for the 2s Lamb shift]

$$\Delta E_{2p_{1/2}-2p_{3/2}}^{\text{Tot,fs}}(R) = 8.352051651 - 0.00005203798087 R^2$$
$$+ 1.215060759 \times 10^{-7} R^3$$
$$- 1.544056441 \times 10^{-9} R^4 \text{ meV}. \tag{115}$$

Martynenko [109] found $E_{2p_{1/2}-2p_{3/2}}^{\text{Tot,fs}} = 8.352082$ meV for the fine structure.

A number of terms not included in Eqs. (114) are presented in Table II together with the relevant references. Combining Eq. (114) with the sum of the contributions contained in Table II, I obtain the final $2s - 2p_{1/2}$ energy

$$\Delta E_{2s_{1/2}-2p_{1/2}}^{\text{Tot,fs}}(R)$$
$$= 206.0465137 - 5.226988356 R^2 + 0.03530609322 R^3$$
$$+ 0.00006821634516 R^4 - 5.535529372 \times 10^{-8} R^5$$

$$+ 0.0002962967640 R^2 \ln(R)$$
$$- 0.00004751147090 R^4 \ln(R) \text{ meV}. \tag{116}$$

This can be compared with the result from from Borie [74]

$$\Delta E_{2s_{1/2}-2p_{1/2}}^{\text{Borie,fs}}(R) = 206.0579(60) - 5.22713 R^2$$
$$+ 0.0365(18) R^3 \text{ meV}, \tag{117}$$

and Carroll *et al.* [121]

$$\Delta E_{2s_{1/2}-2p_{1/2}}^{\text{Carlsonfs}}(R) = 206.0604 - 5.2794 R^2 + 0.0546 R^3 \text{ meV}. \tag{118}$$

An extra recoil contribution is given in Ref. [76] for the fine structure, corresponding to entry #9 in Table II for the Lamb shift

$$\Delta E_{2p_{1/2}-2p_{3/2}}^{\text{VPRec.}} = -0.00006359 \text{ meV}. \tag{119}$$

This term corresponds to corrections beyond the full Dirac term. This leads to the final result

$$\Delta E_{2p_{1/2}-2p_{3/2}}^{\text{Tot,fs}}(R) = 8.351988061 - 0.00005203798087 R^2$$
$$+ 1.215060759 \times 10^{-7} R^3$$
$$- 1.544056441 \times 10^{-9} R^4 \text{ meV}. \tag{120}$$

TABLE II. Contributions to the Lamb shift not included in Eq. (114) (meV). The uncertainty on the proton polarization value used in Ref. [12] has been increased by a factor of 10, according to the discussion in Ref. [27].

#	Contribution	Ref.	Value	Unc.
1	NR three-loop electron VP [Eqs. (11), (15), (18), and (23)]	[77]	0.00529	
2	Virtual Delbrück scattering (2:2)	[79,82]	0.00115	0.00001
3	Light-by-light electron loop contribution (3:1)	[79,82]	−0.00102	0.00001
4	Mixed self-energy vacuum polarization	[36,88,110]	−0.00254	
5	Hadronic vacuum polarization	[111–113]	0.01121	0.00044
6	Recoil contribution Eqs. (82) and (83)	[11,37,66,89]	0.05747063	
7	Relativistic recoil of order $(Z\alpha)^5$ Eq. (84)	[11,38–40,42]	−0.04497053	
8	Relativistic recoil of order $(Z\alpha)^6$ Eq. (86)	[11,38]	0.0002475	
9	Recoil correction to VP of order m/M and $(m/M)^2$ in Eq. (4)	[76]	−0.001987	
10	Proton self-energy	[36,38,42,114]	−0.0108	0.0010
11	Proton polarization	[19,38,112,115,116]	0.0129	0.0040
12	Electron loop in the radiative photon of order $\alpha^2(Z\alpha)^4$	[102,117–119]	−0.00171	
13	Mixed electron and muon loops	[120]	0.00007	
14	Rad. recoil corr. $\alpha(Z\alpha)^5$	[65]	0.000136	
15	Hadronic polarization $\alpha(Z\alpha)^5 m_r$	[112,113]	0.000047	
16	Hadronic polarization in the radiative photon $\alpha^2(Z\alpha)^4 m_r$	[112,113]	−0.000015	
17	Polarization-operator-induced correction to nuclear polarizability $\alpha(Z\alpha)^5 m_r$	[113]	0.00019	
18	Radiative-photon-induced correction to nuclear polarizability $\alpha(Z\alpha)^5 m_r$	[113]	−0.00001	
	Total		0.0256	0.0041

B. Transitions between hyperfine sublevels

The energies of the two transitions observed experimentally in muonic hydrogen are given by

$$E_{2p_{3/2}}^{F=2} - E_{2s_{1/2}}^{F=1} = \Delta E_{2s_{1/2}-2p_{1/2}} + \Delta E_{2p_{1/2}-2p_{3/2}}$$
$$+ \tfrac{3}{8} E_{\text{hfs}}^{2p_{3/2}} - \tfrac{1}{4} E_{\text{hfs}}^{2s}, \tag{121}$$

and

$$E_{2p_{3/2}}^{F=1} - E_{2s_{1/2}}^{F=0} = \Delta E_{2s_{1/2}-2p_{1/2}} + \Delta E_{2p_{1/2}-2p_{3/2}}$$
$$- \tfrac{5}{8} E_{\text{hfs}}^{2p_{3/2}} + \tfrac{3}{4} E_{\text{hfs}}^{2s} + \delta E_{\text{hfs}}^{F=1}. \tag{122}$$

Here we use the results from [109] for the $2p$ states

$$E_{\text{hfs}}^{2p_{1/2}} = 7.964364 \,\text{meV},$$
$$E_{\text{hfs}}^{2p_{3/2}} = 3.392588 \,\text{meV}, \tag{123}$$
$$\delta E_{\text{hfs}}^{F=1} = 0.14456 \,\text{meV}.$$

Using the results presented above I get

$$E_{2p_{3/2}}^{F=2}(R_Z, R) - E_{2s_{1/2}}^{F=1}(R_Z, R)$$
$$= 209.92441 - 5.2265008R^2 + 0.035090744R^3$$
$$+ 0.000086717722R^4 - 5.5355294 \times 10^{-8} R^5$$
$$+ 0.040533092R_Z + 0.00018596008R R_Z$$
$$+ 0.00026754376R^2 R_Z + 0.000063748539R^3 R_Z$$
$$- 0.00020892783R_Z^2 - 0.00032967277R R_Z^2$$
$$- 0.00014609447R^2 R_Z^2 + 0.000057775798R_Z^3$$
$$+ 0.00014693531R R_Z^3 - 0.000030280142R_Z^4$$
$$+ 0.00029629676R^2\ln(R)$$
$$- 0.000047511471R^4\ln(R) \,\text{meV}. \tag{124}$$

This can be compared with the result from Jentschura [88]

$$E_{2p_{3/2}}^{\text{Jents.,}F=2} - E_{2s_{1/2}}^{\text{Jents.,}F=1} = 209.9974(48) - 5.2262R^2 \,\text{meV}, \tag{125}$$

using the $2s$ hyperfine structure of [41].

For the other transition I obtain

$$E_{2p_{3/2}}^{F=1}(R_Z, R) - E_{2s_{1/2}}^{F=0}(R_Z, R)$$
$$= 229.66162 - 5.2286590R^2 + 0.035952626R^3$$
$$+ 0.000012706037R^4 - 5.5355294 \times 10^{-8} R^5$$
$$- 0.12159928R_Z - 0.00055788025R R_Z$$
$$- 0.00080263129R^2 R_Z - 0.00019124562R^3 R_Z$$
$$+ 0.00062678350R_Z^2 + 0.00098901832R R_Z^2$$
$$+ 0.00043828342R^2 R_Z^2 - 0.00017332740R_Z^3$$
$$- 0.00044080593R R_Z^3 + 0.000090840426R_Z^4$$
$$+ 0.00029629676R^2\ln(R)$$
$$- 0.000047511471R^4\ln(R) \,\text{meV}. \tag{126}$$

Using Eq. (124), a Zemach radius of 1.0668 fm from [41], and the transition energy from [12], I obtain a charge radius for the proton of 0.84091(69) fm in place of 0.84184(69) fm in Ref. [12] and 0.8775(51) fm in the 2010 CODATA fundamental constant adjustment. This is 7.1 σ (using the combined σ) from the 2010 CODATA value. A summary of proton size determinations is presented in Table III and Fig. 14.

X. CONCLUSION

In the present work, I have evaluated finite-size-dependent contributions to the $n = 2$ Lamb shift in muonic hydrogen,

TABLE III. Proton size determinations (fm). e^-p: electron-proton scattering; μH: muonic hydrogen; ChPt: Lattice QCD corrected with Chiral perturbation theory. The values in the four last lines are obtained using the transition frequency from [12]

Hand *et al.* [1]	0.805	$\pm$	0.011	e^-p
Simon *et al.* [2]	0.862	$\pm$	0.012	e^-p
Mergel *et al.* [122]	0.847	$\pm$	0.008	e^-p
Rosenfelder [123]	0.880	$\pm$	0.015	e^-p
Sick 2003 [124]	0.895	$\pm$	0.018	e^-p
Angeli [125]	0.8791	$\pm$	0.0088	e^-p
Kelly [126]	0.863	$\pm$	0.004	e^-p
Hammer *et al.* [127]	0.848			hydrogen, e^-p
CODATA 06 [11]	0.8768	$\pm$	0.0069	Hydrogen, e^-p
Arington *et al.* [55]	0.850			e^-p
Belushkin *et al.* [54] SC approach	0.844	$^{+0.008}_{-0.004}$		e^-p
Belushkin *et al.* [54] pQCD app.	0.830	$^{+0.005}_{-0.008}$		e^-p
Wang *et al.* [128]	0.828			ChPt
Pohl *et al.* [12]	0.84184	$\pm$	0.00067	μH
Bernauer *et al.* [14]	0.879	$\pm$	0.008	e^-p
CODATA 2010 [15,16]	0.8775	$\pm$	0.0051	Hydrogen, e^-p
Adamuščín *et al.* [129,130]	0.84894	$\pm$	0.00690	e^-p
This work (using $R_Z = 1.045$ fm [131])	0.84079	$\pm$	0.00069	μH
This work (using $R_Z = 1.0668$ fm [41])	0.84089	$\pm$	0.00069	μH
Using Jentschura [88]	0.84169	$\pm$	0.00066	μH
Using Borie	0.84232	$\pm$	0.00069	μH

to the fine structure, and to the 2*s* hyperfine splitting. The calculations were performed numerically, to all order in the finite size correction, in the framework of the Dirac equation. High-order size contributions to the Uelhing potential and to higher-order QED corrections have been evaluated. The full dependance of the 2*s* hyperfine splitting on the proton charge distribution and Zemach radius has been evaluated as well.

The discrepancy between the proton size deduced from muonic hydrogen and the one coming from CODATA is slightly enlarged when taking into account all the newly calculated effects. It is changed from 6.9 σ to 7.1 σ.
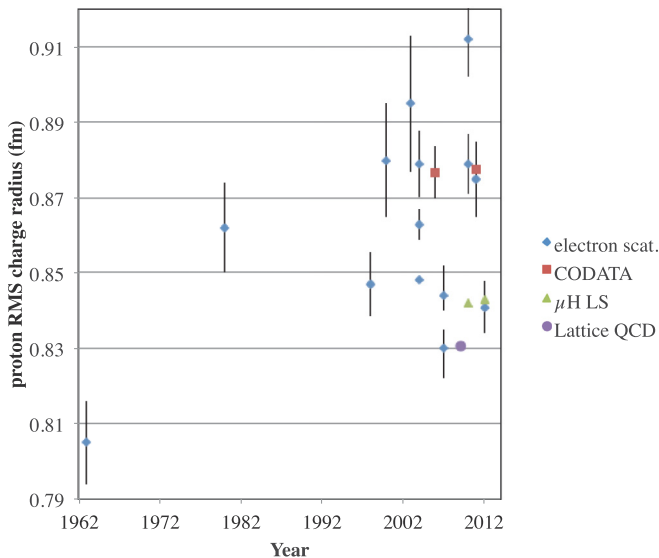

FIG. 14. (Color online) Plot of the proton size as a function of time and method.

APPENDIX A: COEFFICIENTS FOR THE NUMERICAL EVALUATION OF THE KÄLLÉN AND SABRY POTENTIAL FOR A POINT NUCLEUS

The functions defined in Eq. (35) are given here. We find, for $x \leqslant 3$, the functions valid for a point nucleus

$$
\begin{aligned}
g_0(r) = {} & 0.00013575124407339550307 r^8 \\
& - 0.00012633396034194731891 r^7 \\
& + 0.0023754193119115541914 r^6 \\
& - 0.0052460271878852635132 r^5 \\
& + 0.16925588925254111005 r^4 \\
& - 0.25201860708873574898 r^3 \\
& + 0.95109984162919008905 r^2
\end{aligned}
$$

$$- 2.0864972181198001792r$$
$$+ 1.6459704071917522632, \qquad \text{(A1)}$$

$$g_1(r) = -0.00007868467232947335869 r^8$$
$$- 0.0012293141869424835524 r^6$$
$$- 0.097906849416525020713 r^4$$
$$- 0.41666290189975666225 r^2$$
$$+ 0.13769050748433509769, \qquad \text{(A2)}$$

and

$$g_2(r) = -0.000012756169252850100497 r^8$$
$$+ 0.017425498169562658160 r^4$$
$$+ 0.4444444460943167625 \,. \qquad \text{(A3)}$$

For $x > 3$, we fitted the coefficients in Eq. (40) to the numerical values. We obtain

$$a = 4.3942926509010, \quad b = -10.059551479890,$$
$$c = 5.5493632222582, \quad d = 5.3327556570422,$$
$$e = -9.0762837836987, \quad f = 5.1094977559523 \,.$$

Using these functions we reach an agreement to nine decimal place with both the result of the numerical evaluation and the expansion from [72].

APPENDIX B: COEFFICIENTS FOR THE NUMERICAL EVALUATION OF THE KÄLLÉN AND SABRY POTENTIAL FOR A FINITE NUCLEUS

The coefficients for the functions defined in Eq. (39) that we obtained are listed below:

$$h_0(r) = -0.00001608988362060 r^9 + 0.000015791745043 r^8$$
$$- 0.00036443366062 r^7 + 0.0008743378646 r^6$$
$$- 0.038046259798 r^5 + 0.063004651772 r^4$$
$$- 0.36332915853 r^3 + 1.04324860906 r^2$$
$$- 2.39716878893 r + 2.005566300, \qquad \text{(B1)}$$

$$g_1(r) = 0.7511983817345282548$$
$$+ 0.13888763396658555408 r^2$$
$$+ 0.020975409736870016795 r^4$$
$$+ 0.00017561631242035479319 r^6$$
$$+ 9.057708511987165794 \times 10^{-6} r^8, \qquad \text{(B2)}$$

and

$$g_2(r) = -0.4444444460943167625$$
$$- 0.0034850996339125316319 r^4$$
$$- 1.4173521392055667219 \times 10^{-6} r^8 \,. \qquad \text{(B3)}$$

[1] L. N. Hand, D. G. Miller, and R. Wilson, Rev. Mod. Phys. **35**, 335 (1963).

[2] G. G. Simon, C. Schmitt, F. Borkowski, and V. H. Walther, Nucl. Phys. A **333**, 381 (1980).

[3] F. Nez, M. D. Plimmer, S. Bourzeix, L. Julien, F. Biraben, R. Felder, O. Acef, J. J. Zondy, P. Laurent, A. Clairon, M. Abed, Y. Millerioux, and P. Juncar, Phys. Rev. Lett. **69**, 2326 (1992).

[4] M. Weitz, A. Huber, F. Schmidt-Kaler, D. Leibfried, W. Vassen, C. Zimmermann, K. Pachucki, T. W. Hänsch, L. Julien, and F. Biraben, Phys. Rev. A **52**, 2664 (1995).

[5] S. Bourzeix, B. de Beauvoir, F. Nez, M. D. Plimmer, F. de Tomasi, L. Julien, F. Biraben, and D. N. Stacey, Phys. Rev. Lett. **76**, 384 (1996).

[6] A. Huber, T. Udem, B. Gross, J. Reichert, M. Kourogi, K. Pachucki, M. Weitz, and T. W. Hänsch, Phys. Rev. Lett. **80**, 468 (1998).

[7] B. de Beauvoir, F. Nez, L. Julien, B. Cagnac, F. Biraben, D. Touahri, L. Hilico, O. Acef, A. Clairon, and J. J. Zondy, Phys. Rev. Lett. **78**, 440 (1997).

[8] B. de Beauvoir, C. Schwob, O. Acef, L. Jozefowski, L. Hilico, F. Nez, L. Julien, A. Clairon, and F. Biraben, Eur. Phys. J. D **12**, 61 (2000).

[9] M. Niering, R. Holzwarth, J. Reichert, P. Pokasov, T. Udem, M. Weitz, T. W. Hänsch, P. Lemonde, G. Santarelli, M. Abgrall, P. Laurent, C. Salomon, and A. Clairon, Phys. Rev. Lett. **84**, 5496 (2000).

[10] C. G. Parthey, A. Matveev, J. Alnis, B. Bernhardt, A. Beyer, R. Holzwarth, A. Maistrou, R. Pohl, K. Predehl, T. Udem, T. Wilken, N. Kolachevsky, M. Abgrall, D. Rovera, C. Salomon, P. Laurent, and T. W. Hänsch, Phys. Rev. Lett. **107**, 203001 (2011).

[11] P. J. Mohr, B. N. Taylor, and D. B. Newell, Rev. Mod. Phys. **80**, 633 (2008).

[12] R. Pohl *et al.*, Nature (London) **466**, 213 (2010).

[13] J. C. Bernauer, Ph.D. thesis, Johannes Gutenberg Universität, 2010.

[14] J. C. Bernauer *et al.* (A1 Collaboration) Phys. Rev. Lett. **105**, 242001 (2010).

[15] CODATA (2011), http://physics.nist.gov/cuu/Constants/index. html.

[16] P. J. Mohr, B. N. Taylor, and D. B. Newell, Rev. Mod. Phys. **84**, 1527 (2012).

[17] A. De Rújula, Phys. Lett. B **693**, 555 (2010).

[18] A. De Rújula, Phys. Lett. B **697**, 26 (2011).

[19] C. E. Carlson and M. Vanderhaeghen, Phys. Rev. A **84**, 020102 (2011).

[20] C. E. Carlson, V. Nazaryan, and K. Griffioen, Phys. Rev. A **83**, 042509 (2011).

[21] I. C. Cloët and G. A. Miller, Phys. Rev. C **83**, 012201 (2011).

[22] C. Carlson, The European Physical Journal - Special Topics **198**, 65 (2011).

[23] M. O. Distler, J. C. Bernauer, and T. Walcher, Phys. Lett. B **696**, 343 (2011).

[24] G. A. Miller, A. W. Thomas, J. D. Carroll, and J. Rafelski, Phys. Rev. A **84**, 020101 (2011).

[25] I. Sick, Few-Body Syst. **50**, 367 (2011).

[26] M. Vanderhaeghen and T. Walcher, Nuclear Physics News **21**, 14 (2011).

[27] R. J. Hill and G. Paz, Phys. Rev. Lett. **107**, 160402 (2011).

[28] I. Sick, Prog. Part. Nucl. Phys. **67**, 473 (2012).

[29] J. Jaeckel and S. Roy, Phys. Rev. D **82**, 125020 (2010).

[30] V. Barger, C.-W. Chiang, W.-Y. Keung, and D. Marfatia, Phys. Rev. Lett. **106**, 153001 (2011).

[31] B. Batell, D. McKeen, and M. Pospelov, Phys. Rev. Lett. **107**, 011803 (2011).

[32] P. Brax and C. Burrage, Phys. Rev. D **83**, 035020 (2011).

[33] J. I. Rivas, A. Camacho, and E. Göklü, Phys. Rev. D **84**, 055024 (2011).

[34] D. Tucker-Smith and I. Yavin, Phys. Rev. D **83**, 101702 (2011).

[35] V. Barger, C.-W. Chiang, W.-Y. Keung, and D. Marfatia, Phys. Rev. Lett. **108**, 081802 (2012).

[36] K. Pachucki, Phys. Rev. A **53**, 2092 (1996).

[37] A. Veitia and K. Pachucki, Phys. Rev. A **69**, 042501 (2004).

[38] K. Pachucki, Phys. Rev. A **60**, 3593 (1999).

[39] M. I. Eides, H. Grotch, and V. A. Shelyuto, Phys. Rep. **342**, 63 (2001).

[40] E. Borie, Phys. Rev. A **71**, 032508 (2005).

[41] A. P. Martynenko, Phys. Rev. A **71**, 022506 (2005).

[42] M. I. Eides, H. Grotch, and V. A. Shelyuto, *Theory of Light Hydrogenic Bound States*, Springer Tracts in Modern Physics, Vol. 222 (Springer, Berlin, 2007).

[43] D. J. Hylton, Phys. Rev. A **32**, 1303 (1985).

[44] P. Indelicato and J. Desclaux, http://dirac.spectro.jussieu.fr/mcdf (2005).

[45] J. P. Santos, F. Parente, S. Boucard, P. Indelicato, and J. P. Desclaux, Phys. Rev. A **71**, 032501 (2005).

[46] I. P. Grant, Proc. Phys. Soc. London **86**, 523 (1965).

[47] I. P. Grant, Adv. Phys. **19**, 747 (1970).

[48] J. P. Desclaux, D. F. Mayers, and F. O'Brien, J. Phys. B **4**, 631 (1971).

[49] J. P. Desclaux, Comput. Phys. Commun. **9**, 31 (1975).

[50] P. Indelicato, O. Gorceix, and J. P. Desclaux, J. Phys. B **20**, 651 (1987).

[51] P. Indelicato and J. P. Desclaux, Phys. Rev. A **42**, 5139 (1990).

[52] J. P. Desclaux, in *Methods and Techniques in Computational Chemistry*, METTEC, Vol. A: Small Systems, edited by E. Clementi (STEF, Cagliari, Italy, 1993), p. 253.

[53] J. P. Desclaux, J. Dolbeault, M. J. Esteban, P. Indelicato, and E. Séré, in *Computational Chemistry*, Handbook of Numerical Analysis, Vol. X, edited by C. Le Bris and M. De Franceschi (Elsevier, New York, 2003), p. 1032.

[54] M. A. Belushkin, H. W. Hammer, and Ulf-G. Meissner, Phys. Rev. C **75**, 035202 (2007).

[55] J. Arrington, W. Melnitchouk, and J. A. Tjon, Phys. Rev. C **76**, 035205 (2007).

[56] J. L. Friar, Ann. Phys. (NY) **122**, 151 (1979).

[57] H. M. Pilkuhn, *Relativistic Quantum Mechanics*, 2nd ed., Text and Monographs in Physics (Springer-Verlag, Berlin, 2005).

[58] S. J. Brodsky, C. E. Carlson, J. R. Hiller, and D. S. Hwang, Phys. Rev. Lett. **94**, 022001 (2005).

[59] S. G. Karshenboim, Can. J. Phys. **77**, 241 (1999).

[60] S. Klarsfeld, Phys. Lett. B **66**, 86 (1977).

[61] S. Boucard and P. Indelicato, Eur. Phys. J. D **8**, 59 (2000).

[62] E. A. Uehling, Phys. Rev. **48**, 55 (1935).

[63] R. C. Barrett, S. J. Brodsky, G. W. Erickson, and M. H. Goldhaber, Phys. Rev. **166**, 1589 (1968).

[64] L. W. Fullerton and G. A. Rinker, Phys. Rev. A **13**, 1283 (1976).

[65] U. D. Jentschura, Phys. Rev. A **84**, 012505 (2011).

[66] W. A. Barker and F. N. Glover, Phys. Rev. **99**, 317 (1955).

[67] G. Källén and A. Sabry, Det Kongelige Danske Videnskabernes Selskab Matematisk-Fysiske Meddelelser **29**, 3 (1955).

[68] R. Barbieri, J. A. Mignaco, and E. Remiddi, Lett. Nuovo Cimento III **3**, 588 (1970).

[69] R. Barbieri, J. Mignaco, and E. Remiddi, Il Nuovo Cimento A (1971–1996) **11**, 824 (1972).

[70] R. Barbieri, J. Mignaco, and E. Remiddi, Il Nuovo Cimento A (1971–1996) **11**, 865 (1972).

[71] R. Barbieri and E. Remiddi, Il Nuovo Cimento A (1971–1996) **13**, 99 (1973).

[72] J. Blomqvist, Nucl. Phys. B **48**, 95 (1972).

[73] K. P. Burnham and D. R. Anderson, Sociological Methods and Research **33**, 261 (2004).

[74] E. Borie, Ann. Phys. (NY) **327**, 733 (2012).

[75] J. L. Friar and I. Sick, Phys. Rev. A **72**, 040502 (2005).

[76] S. G. Karshenboim, V. G. Ivanov, and E. Y. Korzinin, Phys. Rev. A **85**, 032509 (2012).

[77] T. Kinoshita and M. Nio, Phys. Rev. Lett. **82**, 3240 (1999).

[78] V. G. Ivanov, E. Y. Korzinin, and S. G. Karshenboim, Phys. Rev. D **80**, 027702 (2009).

[79] S. G. Karshenboim, V. G. Ivanov, E. Y. Korzinin, and V. A. Shelyuto, Phys. Rev. A **81**, 060501 (2010).

[80] K. N. Huang, Phys. Rev. A **14**, 1311 (1976).

[81] E. H. Wichmann and N. M. Kroll, Phys. Rev. **101**, 843 (1956).

[82] S. Karshenboim, E. Korzinin, V. Ivanov, and V. Shelyuto, JETP Lett. **92**, 8 (2010).

[83] U. D. Jentschura, P. J. Mohr, and G. Soff, Phys. Rev. Lett. **82**, 53 (1999).

[84] G. W. F. Drake and R. A. Swainson, Phys. Rev. A **41**, 1243 (1990).

[85] U. D. Jentschura, P. J. Mohr, and G. Soff, Phys. Rev. A **63**, 042512 (2001).

[86] P. J. Mohr and G. Soff, Phys. Rev. Lett. **70**, 158 (1993).

[87] P. Indelicato and P. Mohr (private communication, 2012).

[88] U. D. Jentschura, Ann. Phys. (NY) **326**, 500 (2011).

[89] J. R. Sapirstein and D. R. Yennie, in *Quantum Electrodynamics*, edited by T. Kinoshita (World Scientific, Singapore, 1990), pp. 560–672.

[90] G. W. Erickson, J. Phys. Chem. Ref. Data **6**, 831 (1977).

[91] C. Schwartz, Phys. Rev. **97**, 380 (1955).

[92] I. Lindgren and A. Rosén, Case Stud. At. Phys. **4**, 93 (1974).

[93] K. T. Cheng and W. J. Childs, Phys. Rev. A **31**, 2775 (1985).

[94] W. R. Johnson, *Atomic Structure Theory*, Lectures on Atomic Physics (Springer-Verlag, Berlin, 2007).

[95] B. R. Judd, *Operator Techniques In Atomic Spectroscopy*, Princeton Landmarks in Mathematics and Physics (Princeton University Press, Prineton, NJ, 1963).

[96] R. G. Barrera, G. A. Estevez, and J. Giraldo, Eur. Phys. J. D **6**, 287 (1985).

[97] D. A. Varshalovich, A. N. Moskalev, and V. K. Khersonskii, *Quantum Theory of Angular Momentum* (World Scientific, Singapore, 1988).

[98] P. Indelicato, F. Parente, and R. Marrus, Phys. Rev. A **40**, 3505 (1989).

[99] J. E. Rosenthal and G. Breit, Phys. Rev. **41**, 459 (1932).

[100] A. Bohr and V. F. Weisskopf, Phys. Rev. **77**, 94 (1950).

[101] A. J. Freeman, M. Weinert, J. P. Desclaux, and J. V. Mallow, J. Magn. Magn. Mater. **22**, L1 (1980).

[102] E. Borie and G. A. Rinker, Rev. Mod. Phys. **54**, 67 (1982).

[103] A. C. Zemach, Phys. Rev. **104**, 1771 (1956).

[104] G. Breit, Phys. Rev. **35**, 1447 (1930).

[105] E. V. Cherednikova, R. N. Faustov, and A. P. Martynenko, Nucl. Phys. A **703**, 365 (2002).

[106] F. Garcia Daza, N. G. Kelkar, and M. Nowakowski, J. Phys. G: Nucl. Part. Phys. **39**, 035103 (2012).

[107] S. J. Brodsky and G. W. Erickson, Phys. Rev. **148**, 26 (1966).

[108] C. E. Carlson, V. Nazaryan, and K. Griffioen, Phys. Rev. A **78**, 022517 (2008).

[109] A. P. Martynenko, Phys. At. Nucl. **71**, 125 (2008).

[110] U. Jentschura and B. Wundt, Eur. Phys. J. D **65**, 357 (2011).

[111] J. L. Friar, J. Martorell, and D. W. L. Sprung, Phys. Rev. A **59**, 4061 (1999).

[112] A. Martynenko and R. Faustov, Phys. At. Nucl. **63**, 845 (2000).

[113] A. Martynenko and R. Faustov, Phys. At. Nucl. **64**, 1282 (2001).

[114] R. J. Hill and G. Paz, Phys. Rev. Lett. **107**, 160402 (2011).

[115] R. Rosenfelder, Phys. Lett. B **463**, 317 (1999).

[116] A. Martynenko, Phys. At. Nucl. **69**, 1309 (2006).

[117] H. Suura and E. H. Wichmann, Phys. Rev. **105**, 1930 (1957).

[118] A. Petermann, Phys. Rev. **105**, 1931 (1957).

[119] R. Barbieri, M. Caffo, and E. Remiddi, Lett. Nuovo Cimento **7**, 60 (1973).

[120] E. Borie, Helv. Phys. Acta **48**, 671 (1975).

[121] J. D. Carroll, A. W. Thomas, J. Rafelski, and G. A. Miller, Phys. Rev. A **84**, 012506 (2011).

[122] P. Mergell, U. G. Meissner, and D. Drechsel, Nucl. Phys. A **596**, 367 (1996).

[123] R. Rosenfelder, Phys. Lett. B **479**, 381 (2000).

[124] I. Sick, Phys. Lett. B **576**, 62 (2003).

[125] I. Angeli, At. Data Nucl. Data Tables **87**, 185 (2004).

[126] J. J. Kelly, Phys. Rev. C **70**, 068202 (2004).

[127] H. W. Hammer and U.-G. Meißner, Eur. Phys. J. A **20**, 469 (2004).

[128] P. Wang, D. B. Leinweber, A. W. Thomas, and R. D. Young, Phys. Rev. D **79**, 094001 (2009).

[129] C. Adamuščín, S. Dubnička, and A. Z. Dubničková, Nucl. Phys. B, Proc. Suppl. **219-220**, 178 (2011).

[130] C. Adamuscin, S. Dubnicka, and A. Z. Dubnickova, Prog. Part. Nucl. Phys. **67**, 479 (2012).

[131] A. V. Volotka, V. M. Shabaev, G. Plunien, and G. Soff, Eur. Phys. J. D **33**, 23 (2005).